AN ABSTRACT OF THE THESIS OF

Michael R. Kula for the degree of Master of Science in Ocean, Earth, and Atmospheric Sciences presented on June 20, 2017.

Title: The Fully-Coupled One-Dimensional Arctic Surface Energy Budget: Climatology and Projections

Abstract approved:

Justin J. Wettstein

Arctic sea ice concentration and volume have declined due to greenhouse gas radiative forcing and an overall positive climate feedback. At the same time, there have been noteworthy weather and climate circulation anomalies both within the Arctic and extending through the midlatitudes and even into the tropics, leading some studies to conclude that the circulation anomalies are caused by sea ice changes. However, the direct link between sea ice and the atmosphere (i.e. the energy exchange) has not been heavily studied. Our study evaluates the Arctic surface energy budget using a large 33-member ensemble of the fully-coupled Community Earth System Model 1-Community Atmosphere Model version 5 (CESM1-CAM5). From this dataset, mean ensemble trends were calculated from 2011-2040 which is the time period of most severe and consistent sea ice loss. The spatial and seasonal distribution of both the climatology and the trends in the Arctic surface energy budget vary substantially for the radiative and turbulent fluxes (shortwave, longwave, sensible heat, and latent heat), though much of this seasonal and spatial heterogeneity can be understood to coincide with spatial and seasonal changes in sea ice. Four disparate regions stand out and the seasonal dependence of both the

climatology and trend are investigated in detail: the Central Arctic, the Chukchi Sea, the Barents Sea, and the Greenland-Iceland-Norwegian Seas.

Areas with year-round ice coverage in 2040 (i.e. Central Arctic) have a simple energy budget in which shortwave absorption is offset by a steady amount of longwave release throughout the year which does not change much over the course of the 30-year time period of interest. The Chukchi and Barents Seas transition from persistent to marginal and seasonal ice coverage in the projections, resulting in increased summer shortwave absorption that is generally overcompensated primarily via enhanced turbulent heat flux in the late fall and early winter. Marginal sea ice in the northern Greenland-Iceland-Norwegian Seas is effectively removed in the projections, resulting in highly variable but generally strong decreases in the upward turbulent and longwave fluxes as the sea ice is removed even in winter; the strong variability depends on the sea ice distribution projected in each individual ensemble member. Averaged over the whole Arctic, the change in the energy budget is qualitatively similar to that of the Central Arctic: loss of Arctic sea ice results in increased shortwave absorption during the summer which is mostly offset through enhanced longwave release, but how these fluxes are altered is highly geographically and seasonally dependent.

This study strongly suggests that fully-coupled models are essential to recreate physically realistic atmospheric, oceanic, and sea ice conditions as the Arctic continues to experience drastic changes. Drawing physically conclusive links between sea ice concentration declines and impacts on oceanic/atmospheric circulations requires further understanding of the Arctic energy budget, particularly which components are modified and where/when these changes take place with respect to reduced sea ice.

The Fully-Coupled One-Dimensional Arctic Surface Energy Budget: Climatology and Projections

by
Michael R. Kula

A THESIS

submitted to

Oregon State University

in partial fulfillment of
the requirements for the
degree of

Master of Science

Presented June 20, 2017
Commencement June 2018

Master of Science thesis of Michael R. Kula presented on June 20, 2017.

APPROVED:

Major Professor, representing Ocean, Earth, and Atmospheric Sciences

---

Dean of the College of Earth, Ocean and Atmospheric Sciences

Dean of the Graduate School

I understand that my thesis will become part of the permanent collection of Oregon State University libraries. My signature below authorizes release of my thesis to any reader upon request.

Michael R. Kula, Author

ACKNOWLEDGEMENTS

The Author expresses sincere appreciation to Justin J. Wettstein, Emily Shroyer, and Jennifer Hutchings for their guidance throughout this process. Thank you to the fellow CEOAS graduate students (especially my Cascadian cohorts), officemates, Lori Hartline, and Robert Allan.

CONTRIBUTION OF AUTHORS

Justin J. Wettstein assisted with data collection and analysis. Benjamin Lewis and Daniel Watkins assisted with programming. Justin J. Wettstein was involved with the design and writing of this thesis. Justin J. Wettstein, Jennifer Hutchings, and Emily Shroyer also assisted with interpretation of the data.

TABLE OF CONTENTS

LIST OF FIGURES

Figure Page

LIST OF APPENDICES

Chapter 1. Introduction

Motivation

The observed declines in the thickness, concentration and spatial extent of Arctic sea ice are almost universally expected to continue over the coming decades in response to greenhouse gas forcing and climate feedbacks. The loss of Arctic sea ice is most prominent in the late summer and early fall, but large changes in the high-latitude energy budget and its component fluxes will be affected throughout the annual cycle. Such fundamental alterations of the surface energy budget can have far-reaching implications on many other systems (such as feedbacks on sea ice loss, ocean heat content, and oceanic and atmospheric circulations), but very large uncertainties remain regarding which processes dominate the distribution of seasonal and spatial heating and cooling in the Arctic. This study describes some key features in the seasonal and spatial structure of the Arctic energy budget via a detailed one-dimensional energy budget analysis using a large ensemble of fully-coupled climate simulations. This one-dimensional analysis of changes in energy flux is valuable not only in its own right to understand the robustness of seasonal and spatial changes, but as an insight into regions most affected by a changed atmosphere and ocean heat content.

Recent studies have shown that sea ice can strongly influence the surface energy fluxes over the Arctic, with potentially cascading effects on the large-scale atmospheric circulation. The loss of sea ice and consequent open water results in more shortwave absorption as well as alterations in the upward flux of energy including longwave emission and sensible and latent heat release. The alterations in this upward energy flux can have drastic impacts on atmospheric circulations. Deser et. al (2012) found that sea ice extent had a fairly large impact on surface temperatures, precipitation, and snow depth. The loss of sea ice (and the resulting

increase in absorbed shortwave radiation), in conjunction with increased greenhouse gas concentrations, is expected to lead to increased temperatures throughout the year and across almost the entire spatial domain. These increased temperatures (and shortwave absorption) would result in higher water vapor content and low-pressure disturbances which would drive increased precipitation and consequently deeper snow depths. Francis and Vavrus (2012) found that Arctic amplification weakens zonal flow in the upper-portions of the atmosphere and led to "northward elongation of ridge peaks in 500 hPa waves" (Vavrus and Francis, 2012). Both of these impacts would slow the progression of midlatitude storm systems, increasing the chances of extreme instances of droughts, floods, cold outbreaks, and heat waves.

While there are many remaining research questions, these studies highlight the need to further understand the energy budget in the Arctic and how the fluxes in this budget can be expected to change as the loss of sea ice continues in the coming decades. Due to the complexity in feedbacks and forcing between the atmosphere, ocean, and sea ice, and because the ocean modulates the seasonally-dependent atmospheric response to changes in sea ice, it is necessary to evaluate and try to interpret the fully-coupled, energy budget. There has been relatively little explanation of this complex system that utilizes a model that fully incorporates all components. This study helps to fill this research gap. The one-dimensional Arctic surface energy budget is investigated over a thirty-year time interval during rapid Arctic sea ice loss in a thirty-three member ensemble of a state-of the-art fully-coupled model. This climate model has reasonable Arctic sea ice distributions and can therefore be used to interpret the signature of Arctic sea ice loss in the changed surface energy budget terms.

Arctic Energy Budget: Prior Observational Studies

An early but comprehensive assessment of the Arctic energy balance was performed by Oort (1974) using radiosonde data binned into 11 height levels from over 200 stations spanning a 5-year time period. This early study established an analysis framework for the Arctic energy balance. He found that approximately three-quarters of the energy necessary to reach equilibrium (for the atmospheric energy balance) were advected into the Arctic via atmospheric processes while the other quarter was comprised of heat released via sensible/latent heat exchange at the surface. Latent heat transport was found to play a minimal role in comparison to the influx of sensible heat and geopotential (i.e. dry static energy). There were substantial variations in the Arctic energy budget on a year-to-year basis and particularly associated with anomalous advection of dry static energy. Satellite data and a basic atmospheric circulation model was used in conjunction with rawinsonde data to develop a more complete energy budget for the region about a decade later (Nakarmura and Oort, 1988). A key feature of this later study was their analysis of differences in the Arctic and Antarctic energy budgets. They found that the heat exchange between the atmosphere and the ocean-cryosphere played a larger role in maintaining the climatological energy budget in the Arctic than it did in the Antarctic.

Serreze et. al (2007) evaluated the Arctic energy budget using the European Centre for Medium Range Weather Forecasts ERA-40 and National Center for Environmental Prediction (NCEP)/National Center for Atmospheric Research (NCAR) NCEP reanalyses. The net surface fluxes drive the cycle of internanual atmospheric energy storage in this region and play the primary role in altering the amount of atmospheric energy storage over the Arctic. During the spring and summer, the net addition of energy to the surface is used to melt sea ice and the remainder is stored in the ocean. Stored energy is not released until the fall/winter when the downward flux of solar radiation decreases to zero, the atmosphere cools, and the ocean is

thereby able to release a large amount of energy via retarded sea ice growth and the release of sensible/latent heat to the atmosphere. Serreze also examined the contribution of ocean heat transport. He found it to be important in some regions, but it did not contribute meaningfully to the surface energy budget of the Bering Strait or the Fram Strait. Comparisons between the reanalyses and satellite measurements revealed large discrepancies in the net surface fluxes and the top of the atmosphere radiation, casting some doubt on the overall interpretability of the results. Comprehensive satellite observations of all components of the Arctic surface energy budget are notoriously and persistently challenging, especially in the polar night and especially in cloudy sky and other meteorological conditions.

Arctic Energy Budget: Prior Modeling Studies

The sparseness of observational data in the Arctic and the fact that the most extreme Arctic Sea ice loss is likely yet to come enhance the relatively utility of computer models. Ebert et. al (1993) developed and analyzed a one-dimensional model of sea ice that linked thermodynamic and turbulent heat fluxes from the ocean/ice surfaces to the atmosphere. They found that ice thickness was mostly impacted by downward longwave and shortwave radiation and local temperature and humidity. Ocean heat content was only a minor contributor to melting sea ice. Through this model Ebert was able to identify six various feedback loops that impacted sea ice loss: the surface albedo feedback, the conduction feedback, the lead solar flux feedback, the lead fraction feedback, the outgoing longwave flux feedback, and the turbulent flux feedback. Many of these feedbacks play pivotal roles in the enhanced warming of the Arctic. The surface albedo feedback is a positive feedback in which decreased sea ice extent leads to increased shortwave absorption which results in heating of surface waters and enhanced melting of sea ice.

The lead solar feedback is another positive feedback, in which increased shortwave radiation at the surface heats water beneath the ice, which melts ice and decreases ice thickness, thus increasing the amount of shortwave absorption beneath the ice. These positive feedbacks are counteracted by negative feedbacks such as the turbulent flux feedback, whereby surface warming leads to less downward fluxes/more upward fluxes which decreases the net flux at the surface (leading to surface cooling). Although the focus of this study was on the mechanisms leading to ice loss and the subsequent feedbacks the identified processes are relevant for our examination.

There have been a variety of studies using atmosphere-only models. Deser et. al (2010) investigated how the atmosphere responded to a loss of sea ice using an atmospheric general circulation model with an embedded land surface model. This investigation utilized the third generation of the National Center for Atmospheric Research's (NCAR) Community Atmosphere Model (CAM3) and Community Land Models (CLM3). This CAM3/CLM3 model was driven by both control sea ice and sea surface temperatures (SSTs) as well as an experiment that prescribed reductions in sea ice and changes in SSTs. A distinct lag is consistently simulated between the timing of the prescribed sea ice loss and the response of the net surface energy flux; Arctic sea ice loss was simulated to be the largest in September and October but the net surface energy flux peaked a few months later during the late fall and early winter, consistent with the findings by Serreze et. al (2007). Turbulent (latent and sensible heat) fluxes from the ocean to the atmosphere are strongest when the temperature and moisture gradients between the ocean surface and the atmosphere are greatest and when the winds are the strongest, according to the bulk aerodynamic formulae. Semmler et. al (2012) used the EC-EARTH-IFS atmospheric general circulation model with prescribed SSTs and sea ice concentrations to study the impact that

reduced sea ice cover would have on the energy budget of the Arctic as well as climate in the midlatitudes. Decreased sea ice cover had generally large impacts that varied substantially on a seasonal basis. Reduced sea ice cover resulted in increased shortwave absorption and reduced northwards atmospheric energy transport during the summer. During winter, decreased snow cover was simulated to increase upward longwave emission, turbulent energy transfer from the ocean to the atmosphere, and wintertime precipitation. The annual average net surface energy loss declined by about 10 $\frac{W}{m^2}$ poleward of 70 degrees North.

Advances in computer power and the physical realism of computer models have allowed for the development and analysis of fully-coupled models. Sorteberg et. al (2007) examined the Arctic surface energy budget using twenty coupled climate models from fifteen international modeling centers. Sorteberg not only compared the models to NCEP/ERA40 reanalyses and satellite data, but also evaluated the twenty-first century changes in the Arctic surface energy budget. Sorteberg identified numerous inconsistencies between the models and satellite-based reanalysis-based calculations; most models underestimated both upward and downward longwave radiation in winter and net downward shortwave radiation in both summer and autumn but overestimated net downward solar radiation in spring. The models faithfully simulated that increases in sea ice loss resulted in decreased amounts of upward (reflected) shortwave radiation due to the lowered albedo. Increased surface temperatures caused larger outgoing longwave radiation. Overall, the net surface radiation budget changed by 5.8 $\frac{W}{m^2}$ averaged over the Arctic poleward of 70 degrees North over the course of the year, with most of this net energy addition being offset by increased amounts of sensible and latent heat flux from the surface to the atmosphere. Krikken and Hezeleger (2015) also investigated the Arctic surface energy budget in fully-coupled simulations, but from the updated Coupled Model Intercomparison Project Phase 5

(CMIP5) database. The authors found that the primary role of the ocean is to store heat anomalies in the spring and release them later in the year during the fall while ocean heat flux variations are fairly minor. They also found that spring sea ice anomalies do not generally result in immediate cloud changes or responses in other aspects of the atmosphere, but there is a delayed response in fall. In addition to results that are broadly consistent with the seasonally delayed response in other studies (although a bit earlier), they found that the cloud and ice-albedo feedbacks are realized most strongly during the fall in most models.

Sea Ice Polar Amplification and the Subpolar Atmospheric Circulation

There are a large number of studies that have investigated the covariability of Arctic Sea ice extent and/or polar amplification and the weather and climate in both the Arctic and the subpolar midlatitudes. One of the first studies conducted that identified a link was conducted by Overland et. al (1981). Using monthly maps, the authors developed a 23-year long climatology of storm tracks in the Bering Sea. Comparing the storm tracks between low-ice extent years to high-ice extent years showed some very definitive differences. Storms in low-ice extent years tended to travel along the western portion of the Bering Sea while storms in high extent years propagated along the eastern portion of the Sea. This led the authors to conclude that extratropical cyclones were the primary factor in determining the variability in sea ice extent in the Bering Sea. This study demonstrates that atmosphere-ice covariability can be driven fundamentally by atmospheric, rather than sea ice, variability.

Numerous studies have found a link between sea ice concentration and the atmospheric phenomenon known as the North Atlantic Oscillation (NAO). Magnusdottir et. al (2004) found that sea ice concentration is a generally more effective forcing than sea surface temperature

anomalies in terms of driving the NAO response in an NCAR atmospheric general circulation model (Community Climate Model 3) with specified SSTs and sea ice concentrations. The authors found that sea ice declines resulted in an atmospheric response that resembled the negative phase of the NAO. Alexander et. al (2004) found that areas with sea ice loss are often simulated to have large changes in both the thermodynamic fluxes and conditions of the atmospheric boundary layer using an atmospheric model with prescribed sea ice coverage. The changes included large upward surface heat fluxes, near-surface warming, enhanced precipitation, and below-normal sea level pressure where the prescribed sea ice was diminished and opposite changes where it was prescribed to expand. Alexander also found that the strength of the atmospheric response scales with the amount of sea ice loss, thus this sea ice forcing could become more severe if Arctic Amplification continues due to growing greenhouse gas concentrations. Seierstad and Bader corroborated these findings in 2008 by using an atmospheric model (ECHAM5) and prescribed only idealized reductions in sea ice. They found that significant reductions in midlatitude and Arctic storminess were associated with an atmospheric response that resembles the negative phase of the North Atlantic Oscillation and corresponding projection for weaker, southward-shifted, and more zonal storm tracks. All of these atmosphere-only modeling studies focused on one of the consistently strongest atmospheric responses to sea ice loss – a negative NAO response that occurred in winter.

Vavrus and Francis (2012) studied how Arctic Amplification could be impacting 500 hPa geopotential heights and corresponding weather conditions in the Arctic and subpolar midlatitudes using an NCEP/NCAR reanalysis dataset. The authors found that the warming in the Arctic coincided with a reduced gradient in the 1000-500hPa thicknesses in the midlatitudes as well as northward elongation of midlatitude ridge peaks for waves identified in the 500 hPa

geopotential height field. Both of these alterations are consistent with reduced zonal flows which means waves will propagate eastward at a slower pace. Slower moving waves could result in more instances of extreme weather such as floods, droughts, heat waves, and cold spells due to this now prolonged (and perhaps more intense) exposure to synoptic-scale disturbances. The authors postulate that this alteration in wave speed and structure was caused by Arctic Amplification and could be responsible for some of the more recent severe weather events such as the cold and snowy winters of 2009-10 and 2010-11 in eastern United States and Europe, the historic heat-wave and drought in Texas during 2011, and the record-breaking rainfall in the northeast United States during the summer of 2011. Liu et. al (2012) also identified links between Arctic sea ice loss and both precipitation patterns and cold air outbreaks. The authors analyzed a combination of satellite observations, ground monitoring stations, and reanalysis data in an attempt to quantify the strength of this connection between extreme midlatitude weather and sea ice loss. The authors ultimately concluded that sea ice loss could have been responsible for the cold and snowy winters of 2009-10 as well as 2010-11 in North America and Europe. Deser et. al (2010), mentioned previously, also found that sea ice greatly impacted surface temperature, precipitation, and snow cover, especially on Arctic land areas near the prescribed sea ice reductions. All of these factors would act to decrease the static stability in the boundary layer by ~50%. Peings et al. (2013) found that current ice conditions (as well as decreased ice concentrations in the future) favored or were associated with drastic cold air outbreaks in the midlatitudes using the Community Earth System Model-Community Atmosphere Model 5 (CESM1-CAM5). Deser et. al (2015), using the Community Climate System Model version 4 (CCSM4), investigated how Arctic sea ice loss and ocean coupling can impact the atmosphere. Without ocean coupling, the atmospheric responses to Arctic sea ice loss are confined to a

boundary north of 30 degrees North with weakened westerlies that shift towards the equator, warming in the lower troposphere, and increased precipitation in the high latitudes. With ocean coupling, the atmospheric response covers the entire globe, acts to warm the entire troposphere, and increases the strength of the extratropical northern hemisphere zonal winds by 30% when compared to the models without ocean coupling. Furthermore, ocean coupling also strengthens the hydrological cycle and shifts the intertropical convergence zones to the equator. Blackport and Kushner (2016) altered the albedo of sea ice to investigate the impact that sea ice loss would have on atmospheric circulations using CCSM4. Their findings generally corroborated the work of Deser et. al (2010), where the largest atmospheric responses are being realized in the fall and winter. However, the transient response is small and the atmospheric general circulation response is very weak. Once the sea ice melts, the variability in the surface temperatures in the Arctic diminishes due to decreased temperature gradients and the moderating influences of the open ocean. Tomas et. al (2016) used CCSM4 to evaluate how thermodynamic and dynamic coupling can impact atmospheric responses. When dynamic coupling is removed the atmospheric response is asymmetric, with maximum warming occurring at the high northern latitudes that decreases towards the equator which displaces the ITCZ and Hadley cell circulation northward. With both dynamic and thermodynamic coupling, the response is symmetrical: warming occurs at the upper latitudes in both hemispheres and along the equator due to anomalous ocean heat content transport convergence. This convergence also acts to intensify the northern and southern branches of the ITCZ. The strengthening of the ITCZ and the subsequent changes in SST-precipitation in the Pacific results in atmospheric circulations and teleconnections that drive Rossby waves to the midlatitudes in both hemispheres.

Complexity and the Need for a Refined Physical Understanding

The aforementioned links between Arctic sea ice, the Arctic energy budget, and especially the attribution of subpolar weather impacts to polar climate change are not universally accepted. One of the aforementioned studies (Semmler 2012) argued that sea ice loss lowered the chances for cold events and precipitation in the northern midlatitudes while numerous authors such as Liu, Peings, and Vavrus and Francis argue the opposite. Overland et. al (1981) found that the atmosphere played the primary role in driving interannual variability in sea ice extent, yet almost all of the aforementioned argued the opposite: that the sea ice drove an important atmospheric response. Other studies have been more direct in their criticisms regarding linking sea ice and atmospheric circulation anomalies. Barnes (2013) found issues regarding the methodology and physical interpretability of results in previous studies that linked Arctic Amplification to extreme subpolar weather, especially Vavrus and Francis (2012). Barnes conducted a study using four modern reanalyses to test this link and found that the methodology does not adequately represent the dynamics of the proposed response and that the actual data implies no coherent link between sea ice cover and extreme weather occurrences in the northern midlatitudes. Sorokina et. al (2016) also found that the coupled atmosphere-ocean-sea ice system is much more complex than the uncoupled atmosphere-only simulations suggests and the interannual variability in sea ice loss over the winter Barents Sea was associated with reduced (not increased) turbulent heat fluxes as both the heat flux and sea ice reduction itself were dominated by passing baroclinic waves (i.e. by anomalous atmospheric circulation).

Our Study

As detailed above, Arctic sea ice loss has an important influence on the surface energy budget with potential impacts on atmospheric and oceanic circulations. This region has been heavily studied in regards to its energy budget and covariance between Arctic Amplification and the atmosphere structure as well as weather and climate variability patterns. However, understanding the specific linkage between sea ice and the atmosphere requires a detailed understanding of the distinct changes to the Arctic surface energy budget and how the terms of this budget, in particular the turbulent heat fluxes, are going to change. This investigation will help isolate the realistic atmospheric response in a fully-coupled investigation and isolate it from other broader changes that could result from greenhouse gas forcing and the associated feedbacks or from circulation changes that are predominantly driven from outside the Arctic. The complex interactions between the atmosphere, ocean, and sea ice identified in several previous studies suggests the need for the investigation of a coupled system that incorporates all important interactions instead of essentially prescribing them. Sorteberg et. al (2007) evaluated the surface energy budget and assessed the implications to sea ice loss in a fully-coupled modeling framework, but the climatology and projections of the CMIP3-era coupled climate models were notoriously unrealistic (e.g. Stroeve et. al, 2007). This study will evaluate the one-dimensional Arctic surface energy budget in a large ensemble from a state-of-the-art, fully-coupled climate model with realistic Arctic sea ice (Jahn et. al, 2012). This analysis will identify particular structures in the seasonal and spatial projected changes in the Arctic surface energy budget and tie them to the physical response to continued decline in sea ice extent. The seasonal and spatial structures of Arctic energy budget changes are largely absent in the previous studies that correlate midlatitude anomalies with pan-Arctic sea ice change and are unrealistic in the

atmosphere-only experiments that prescribe sometimes unphysical seasonal and spatial distributions of sea ice loss.

Chapter 2. Data and Methods

CESM1-CAM5 Model Overview

Accurately representing the fully-coupled Arctic energy budget requires a model which incorporates the complex interactions between the atmosphere, sea ice, and at least the surface ocean. A large (33-member) initial condition ensemble from the Community Earth System Model version 1 (CESM1) with the Community Atmosphere Model version 5 (i.e CESM1-CAM5) was chosen for this study. The successor to the Community Climate System Model (CCSM), CESM1-CAM5 is a fully-coupled model that includes component models of the atmosphere, land surface, ocean, land ice, sea ice, vegetation, and related systems. The previous version of CESM1 (CESM1-CAM4) has been shown to successfully represent important characteristics of Arctic sea ice in the late twentieth century such as the spatial distribution of sea ice concentration, sea ice extent, multiyear sea, sea ice thickness patterns, and melt season length (Jahn et. al, 2012).

The thirty-three members of the CESM1-CAM5 ensemble were run forward in time for a 75-year time period from 2006 through 2080 and consistently subjected to the same RCP8.5 emissions scenario that ultimately is related to the amount of additional radiative forcing from greenhouse gas emissions and other anthropogenic causes (Figure 1).

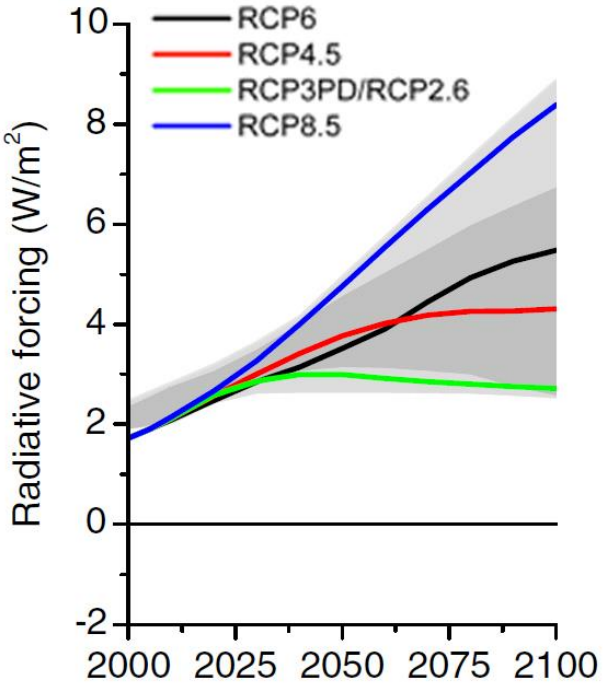

Figure 1: Total radiative forcing for the various RCP scenarios. RCP8.5, the scenario used in this analysis, is in blue. Obtained from IPCC Data Distribution Centre (http://sedac.ipcc-data.org/ddc/ar5_scenario_process/RCPs.html).

The atmospheric component of CESM1 has a latitudinal resolution of .9424 degrees and a longitudinal resolution of 1.25 degrees at 30 different vertical levels that range from the surface to 3 hPA. CAM5 is an upgrade over its predecessor (CAM 4) in several respects. CAM5 is the first atmospheric model from NCAR that is able to realistically simulate cloud-aerosol radiative effects, cloud droplet activation by aerosols, and particle-size dependent precipitation. Also new to CAM5 is the inclusion of a new moist turbulence scheme, a new shallow convection scheme, a revised cloud macrophysics scheme, and a new 3-mode modal aerosol scheme (Neal, 2012). Several of these changes are likely to result in a more faithful simulation of the energy budget and related features like lapse rates and stability over the Arctic.

Cloud conditions over the Arctic are a particular area of improvement. While certain biases remain, CAM5 has made significant improvements in three primary common to many climate model cloud biases: underestimation of total clouds, the overestimation of optically thick clouds, and the underestimation of midlevel clouds (Kay, 2012). All of these will also have a profound effect on the Arctic surface energy budget. The four component fluxes of the net surface energy budget over the Arctic are obtained from the CAM5 component model in CESM1-CAM5 namely: 1) net shortwave flux at the surface (SW), 2) net longwave flux at the surface (LW), 3) net latent heat flux at the surface (LH), and 4) net sensible heat flux at the surface (SH). Furthermore, the net shortwave flux at the top of the atmosphere, the net longwave flux at the top of the atmosphere, surface temperature, and sea level pressure will also be used to qualitatively determine energy storage and transport in the atmosphere.

The oceanic component of CESM, the Parallel Ocean Program (POP), has 60 levels in the vertical with nominally 1° horizontal resolution. The ice concentration data was obtained from CAM5 datafields processed by the model's ocean-atmosphere coupler. The ocean heat content per square meter of sea water was calculated from POP model output over the top 100 meters by multiplying ocean temperature by the vertical depth of the grid cell by the density of sea water and the heat capacity of sea water. 100 meters was chosen as a rough balance between winter and summer mixed layer depths in the Arctic based off previous studies (Peralta-Ferriz & Woodgate, 2015).

The newest version of the Los Alamos Sea Ice Model (CICE4) operates on the same grid and interacts directly with the POP model. Sea ice volume was calculated as the product of the gridcell-average sea ice thickness and the horizontal area of the grid cell using the CICE4 model. Both POP and CICE4 model results were regridded to the CAM5 grid via standard regridding

algorithms developed at NCAR and consistent with the ocean-atmosphere coupler in order to homogenize the calculations of the surface energy flux and ocean and sea ice changes onto a consistent horizontal grid. The last major component of CESM is the Community Land Model, version 4 (CLM). This land surface component model operates on the same grid and interacts with the CAM5 atmospheric component. While this model's output is not a primary concern for this study and will not be evaluated directly, the fully-coupled nature of CESM1-CAM5 means that this model's influence could be a factor in the final results.

Conservation of Energy: The Arctic Surface Energy Budget

The backbone of this study is the conservation of energy: the amount of energy entering a well-defined boundary of a material must equal the amount of energy leaving or otherwise contribute to a change in the energy of the material itself. This means that if there is an imbalance in the radiative and turbulent fluxes (RTF) energy must be either stored or advected. In other words:

$$\frac{dE}{dt} = \frac{dS_{Surface}}{dt} = \Sigma(RTF)_{Surface} + Advection$$

where $\frac{dE}{dt}$ is the change in energy over time; $\frac{dS_{Surface}}{dt}$ is the change in storage related to the ocean heat content and ice melt/warming; $\Sigma(RTF)_{Surface}$ is the sum of the radiative and turbulent fluxes (SW, LW, LH, and SH) at the surface; and $Advection$ refers to the transfer of energy into and out of the system via atmospheric/oceanic currents and sea ice transport. Since energy must be conserved, $\frac{dE}{dt}$ is equal to 0 when averaged over a sufficient duration in an equilibrium climate sate. The above equation can be modified and applied to the surface (skin) of

the Earth to solve for the amount of energy advection, which can then be calculated as the residual from all the RTF terms and different types of storage.

$$Advection = \frac{dS_{Surface}}{dt} - (RTF)_{Surface}$$

The $\Sigma(RTF)$ term is the sum of all the radiative and turbulent fluxes at each particular grid point in the model. The component terms of RTF are net shortwave flux at the surface (SW), net longwave flux at the surface (LW), net latent heat flux at the surface (LH), and net sensible heat flux at the surface (SH). The SW and LW terms are radiative and the LH and SH terms are associated with turbulent fluxes. If the sense of the fluxes is consistently that downward (into the surface) is positive, the sum of the RTF term can be represented mathematically as:

$$(RTF)_{Surface} = SW_{Surface} + LW_{Surface} + SH_{Surface} + LH_{Surface}$$

Given the sign convention above, positive values of RTF components represent energy added to the surface whereas negative values represent energy removed from the surface.

The rate of climatological energy storage in the surface ($\frac{dS}{dt}$) is comprised of two subcomponents, the rate of ocean heat uptake and the net energy required to heat and melt sea ice. Storage is calculated as the change in Arctic ocean heat content at a depth of 100 meters (OHC) which approximates the seasonally varying Arctic mixed layer depth. However, in this study the amount of energy necessary to warm/melt sea ice does not need to be computed, as this energy change is taken into account by alterations in both ocean heat content as well as the radiative and turbulent fluxes (i.e. these terms adjust according to ice growth/melt). Putting all these terms together, the mathematical form of the Arctic surface energy budget becomes

$$\frac{dE_{Surface}}{dt} = \frac{d(OHC)}{dt} = SW_{Surface} + LW_{Surface} + SH_{Surface} + LH_{Surface} + Advection$$

In this study the different pathways in which energy must be entering or exiting a system to equilibrate areas experiencing RTF imbalances will also be qualitatively studied. The energy budget of the atmosphere will also be studied by utilizing the following equation:

$$\frac{dS_{Ats}}{dt} + Transport = SW_{TOA} + LW_{TOA} - \left(SW_{Surface} + LW_{Surface}\right) + SH_{Surface} + LH_{Surface}$$

Due to computational limitations, the exact values for atmospheric storage and transport cannot be directly calculated. The combined terms can be estimated as the residual of the radiative and turbulent energy fluxes at the surface and the TOA. Additional information, such as sea level pressure and surface temperature, will be used in conjunction with the above equation to qualitatively assess the probability of atmospheric storage or transport occurring in a particular area.

Because this study intends to add clarity to how the Arctic energy budget changes in response to changes in Arctic sea ice, a primary consideration is what time interval to evaluate. The total Arctic sea ice area is calculated and plotted for each ensemble members for the months from September to December (Figure 2).

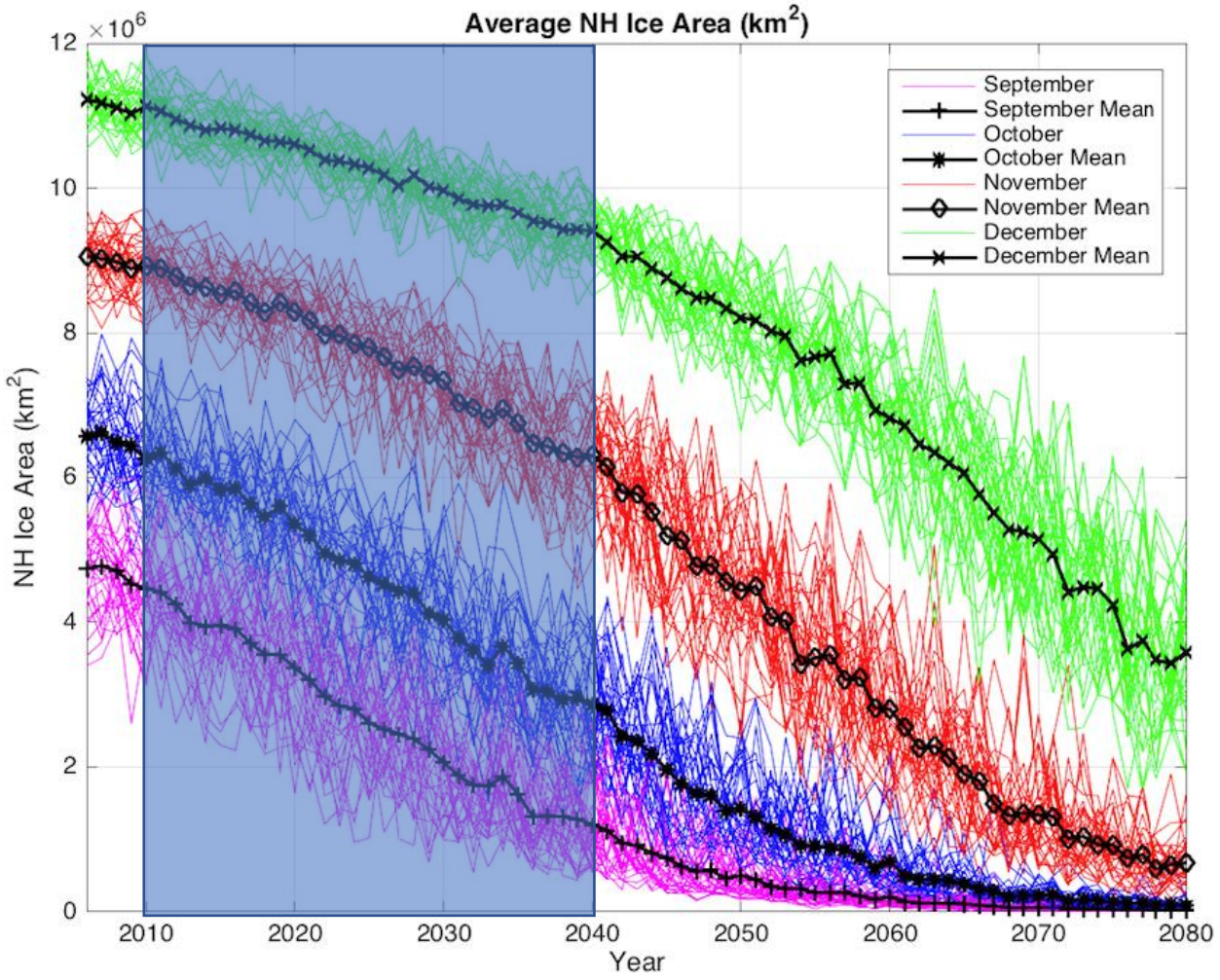

Figure 2: Total sea ice area projections by month for the 33-member CESM1-CAM5 ensemble. The time period between 2010-2040 (shaded above) is the time period that will be examined in this study.

The 2010 and 2040 analysis interval was chosen because it is when sea ice decline is most rapid and uniform. 30-year (2011-2040) trends for this period were calculated at each gridpoint for each of the terms in the Arctic energy budget described previously.

Chapter 3. Results

Sea Ice Decline

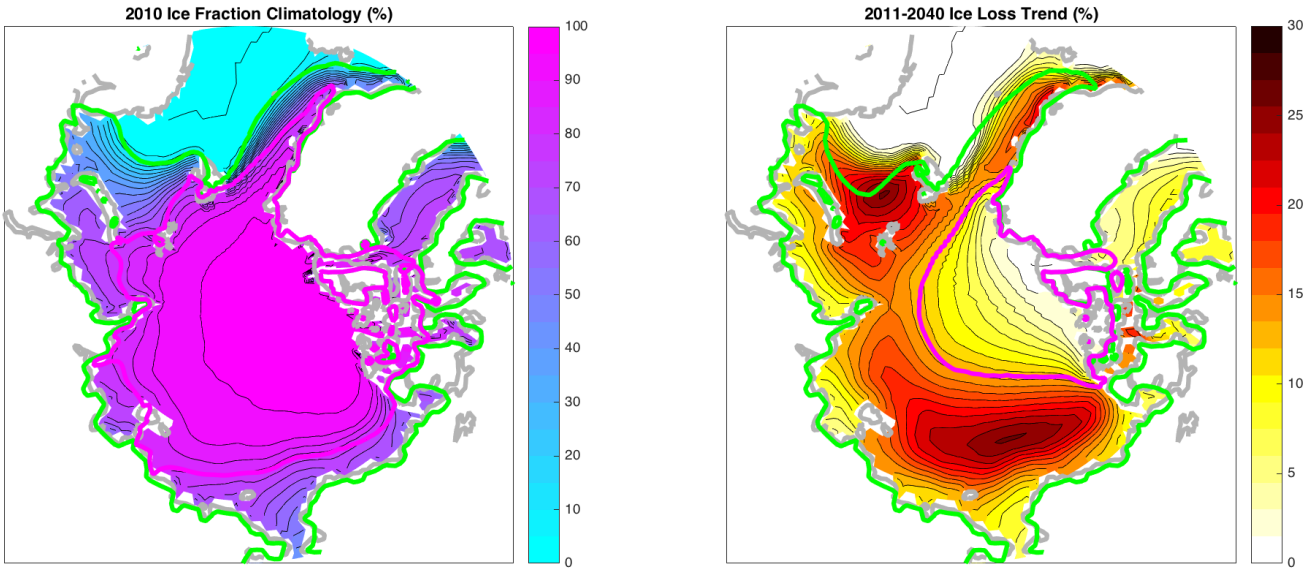

Figure 3: 2010 ensemble-mean ice fraction (A) and 2011-2040 % of sea ice loss (B). Overlying green contours show maximum sea ice extent while overlying pink contours show minimum sea extent in 2010 (left plot) and 2040 (right plot).

Figure 3 shows the 2010 climatology and 2011-2040 trends in sea ice %. The 2010 sea ice shows that the highest concentrations of sea ice are located in the interior of the Arctic ocean and bounded by landmasses such as Greenland and the Canadian Archipelago. Sea ice fraction declines as you move southward, with the lowest concentrations and highest gradients in areas that experience large influences from southerly ocean currents such as the Barents Sea. Sea ice loss during the 30-year time period of interest is greatest in areas that are located on or nearby current marginal ice zones such as the Barents and Chukchi Seas.

Spatial Distribution of RTF Fluxes

The 2010 ensemble mean climatology and the 2011-2040 trends for the various components of the Arctic energy budget are mapped to get a sense of the spatial distribution of

each term's importance in the climatology and projected change. Positive values on these plots are consistent with energy being added to the Earth's surface, while negative values represent energy being removed from the surface.

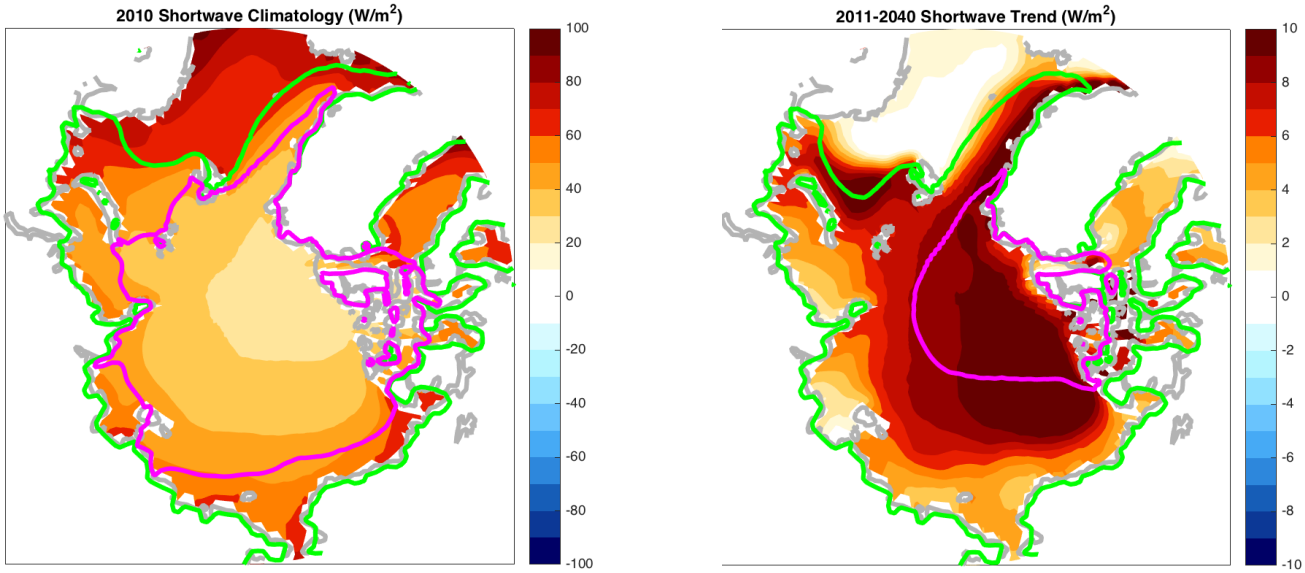

Figure 4: 2010 ensemble-mean climatology (A) and 2011-2040 trend (B) in annual net shortwave flux at the surface. Dotted (solid) green contour shows the 15% ice fraction maximum (minimum) in 2010, while the dotted (solid) pink contour shows the 15% ice fraction maximum (minimum) in 2040.

The shortwave climatology shows a very clear distribution over the Arctic Ocean in which the amount of net downward surface shortwave radiation is strongly related to sea ice concentration distribution. The amount of net downward SW is strongly diminished in regions where there are high sea ice concentrations, such as the Central Arctic. The opposite is also true- areas with marginal or seasonal 2010 sea ice loss (e.g. Barents and Kara Seas) experience increased net downward SW.

Declines in Arctic sea ice extent combined with earlier melt onset during the 2011-2040 interval is expected to result in an almost universal increase in absorbed shortwave radiation throughout the Arctic region, but the distribution of this increase in downwelling (ultimately absorbed) SW is unevenly distributed (Figure 4b). The increased shortwave absorption is largest

in the central Arctic throughout the Canadian archipelago, in the Fram Strait, Barents Sea, and Kara Sea. Much of these locations were projected to gain in excess of 10 W/m^2. These are also the regions where sea ice coverage is expected to decrease the most during the 30-year time period. The Barents Sea experiences a large change in absorbed SW as it is located in the marginal ice zone between the 2010 maximum/minimum sea ice extent in the model, which is broadly consistent with observations that indicated this region is very sensitive to climate change (e.g. it is the region where winter sea ice loss has been most extreme).

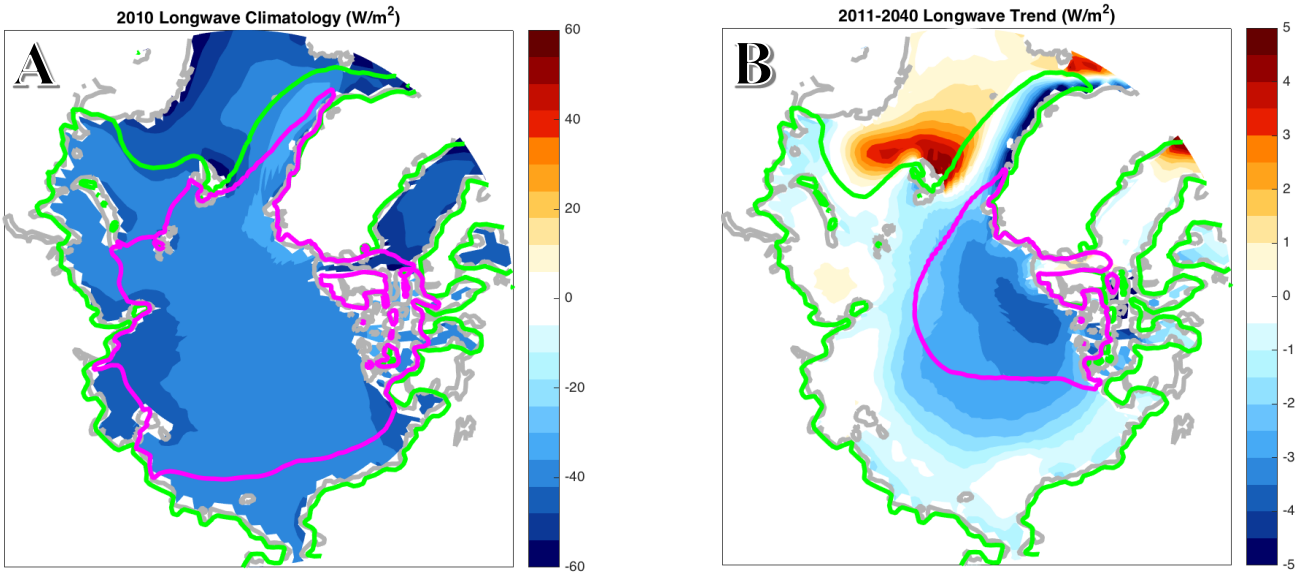

Figure 5: 2010 ensemble-mean climatology (A) and 2011-2040 trend (B) in annual net longwave flux at the surface. Dotted (solid) green contour shows the 15% ice fraction maximum (minimum) in 2010, while the dotted (solid) pink contour shows the 15% ice fraction maximum (minimum) in 2040.

Figure 5 shows the net downward longwave radiation from the surface. In the 2010 climatology (Fig. 4a), the amount of longwave emission is fairly uniform, hovering right around 40-45$\frac{W}{m^2}$ throughout most of the Arctic. The magnitude of the 2011-2040 trend in longwave emission is almost everywhere smaller than the SW trend, but a few aspects of the spatial distribution are worthy of note. The amount of longwave emission from the Earth's surface (i.e. a negative number) over the central Arctic is expected to increase by 3-4$\frac{W}{m^2}$. The Greenland-

Icelandic-Norwegian Seas experience a rather large trend toward increased downward net longwave radiation even though its amount of shortwave absorption is not changing due to its fairly ice-free local. The reasoning behind this anomaly will be discussed further in the discussion. Meanwhile, the Barents Sea, which according to Figure 3b is absorbing much more energy, is actually releasing just about the same amount of energy via longwave emission as it was previously. Considering the energy balance formulation, these final two points make it clear that the other components of the energy budget must be playing a large role in these regions.

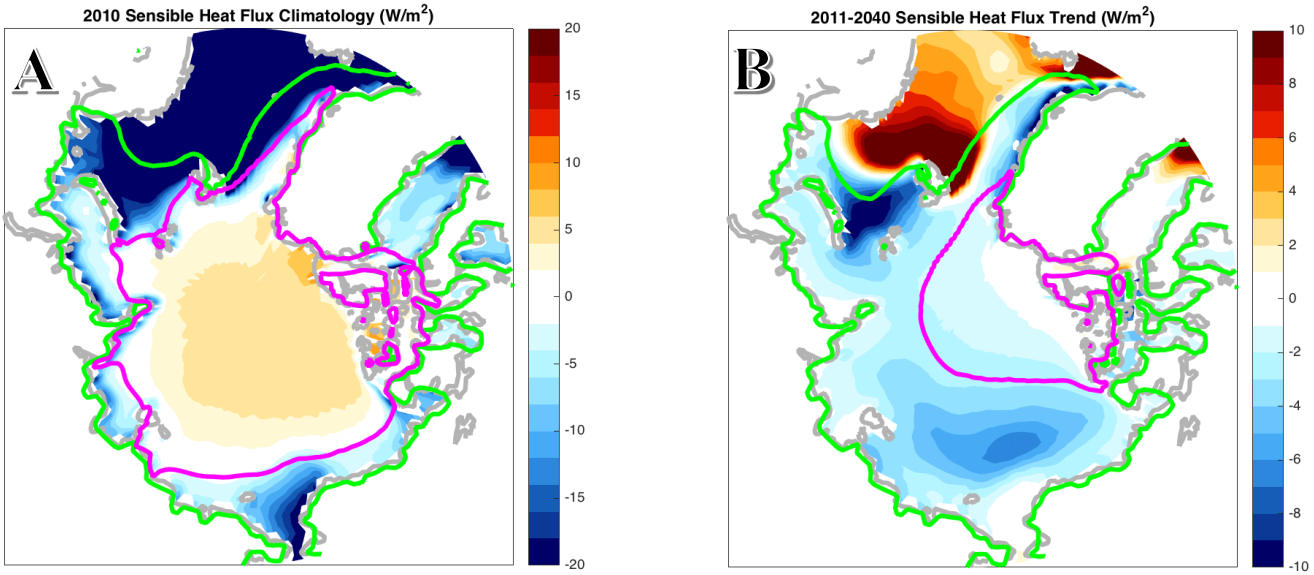

Figure 6: 2010 ensemble-mean climatology (A) and 2011-2040 trend (B) in annual net sensible heat flux at the surface. Dotted (solid) green contour shows the 15% ice fraction maximum (minimum) in 2010, while the dotted (solid) pink contour shows the 15% ice fraction maximum (minimum) in 2040.

Figure 6 shows the 2010 climatology and 2011-2040 trend in net downward sensible heat flux. In the 2010 ensemble-mean climatology there is a clear pattern of sensible heat into the surface in ice covered regions and sensible heat release in ice-free/marginal sea ice zones. In essence, energy in the form of sensible heat was being used to heat ice in areas of high ice-concentration but in ice-free regions the exposed open ocean is able to dump energy due to the cooler overlying air. Sensible heat plays a role in moderating the Arctic energy budget,

especially in regions where 2011-2040 sea ice concentration changes are most prevalent. There is an increase in ocean-to-atmosphere (i.e. a reduction in atmosphere to ocean sensible heat flux) sensible heat flux in the Chukchi Sea, an area over which the maximum sea ice extent changes dramatically (e.g. Deser et. al). There is a very strong dipole signature occurring in the Barents Sea region, with a large increase in net sensible heat flux into (most likely interpretable as a large decrease in sensible heat flux loss) the surface along the current sea ice maximum boundary and a large decrease in the net sensible heat flux into the surface (i.e. a large increase in sensible heat flux lost from the surface) in the area between the minimum ice extent in 2010 and 2040. Based on the location of these large variations in sensible heat flux, it is obvious and not surprising that the presence or absence of sea ice is a critical factor in determining the strength of the sensible heat flux in broad agreement with previous studies (Deser et. al, 2010). The so-called “sea ice edge” commonly associated with the 15% isopleth is a zone of concentrated sensible heat flux loss from the surface to the atmosphere. As the locations of this sea ice edge are projected to change, new areas of large sensible heat flux appear to be created (Chukchi Sea) or the area of intense sensible heat flux seems to move (Barents Sea).

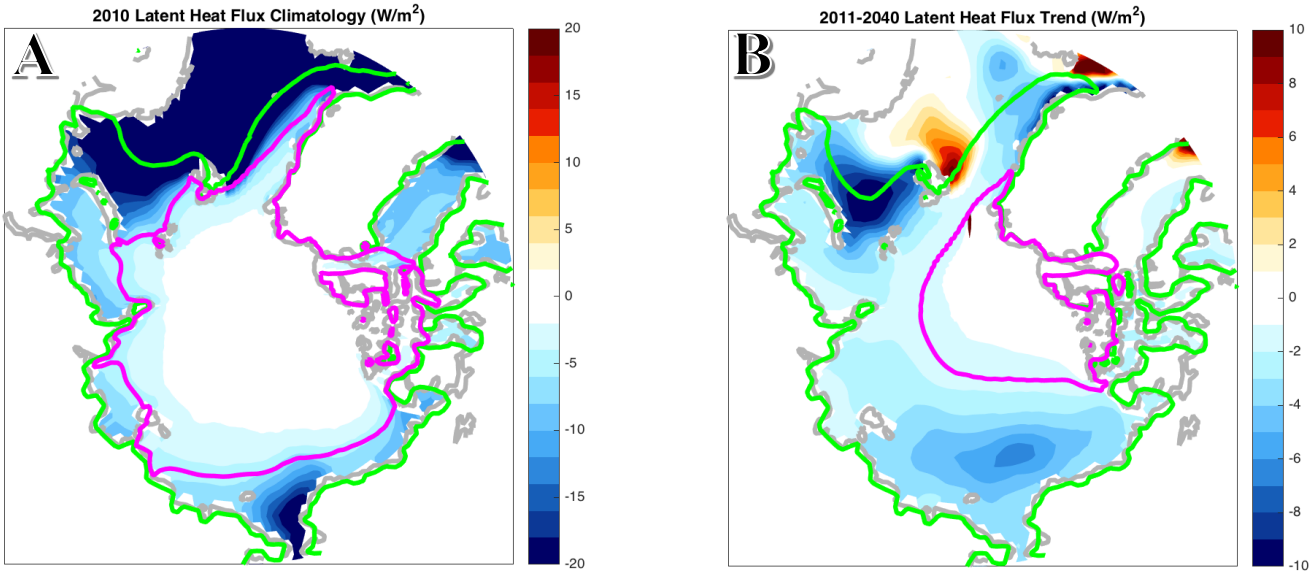

Figure 7: 2010 ensemble-mean climatology (A) and 2011-2040 trend (B) in annual net latent heat flux at the surface. Dotted (solid) green contour shows the 15% ice fraction maximum (minimum) in 2010, while the dotted (solid) pink contour shows the 15% ice fraction maximum (minimum) in 2040.

The spatial distribution of the climatology for the latent heat flux (Fig. 7a) and the 2011-2040 trends for latent heat (Fig. 8b) can be seen above. Latent heat loss is a loss term throughout the whole Arctic Ocean, with the highest values occurring in open ocean/marginal ice zones due to increased temperature/moisture gradients between open water and the atmosphere. Latent heat is essentially a non-contributor in areas with sea ice year-round. The spatial distribution and magnitudes of projected trends for the latent heat flux are broadly similar to those in sensible heat even though the climatology of sensible heat and latent heat are different. A strong dipole in the trend of latent heat flux exists over the Barents Sea much like it did for the sensible heat flux. As with sensible heat flux, the regions experiencing the largest changes in sea ice concentration are those with the most volatile changes in latent heat release.

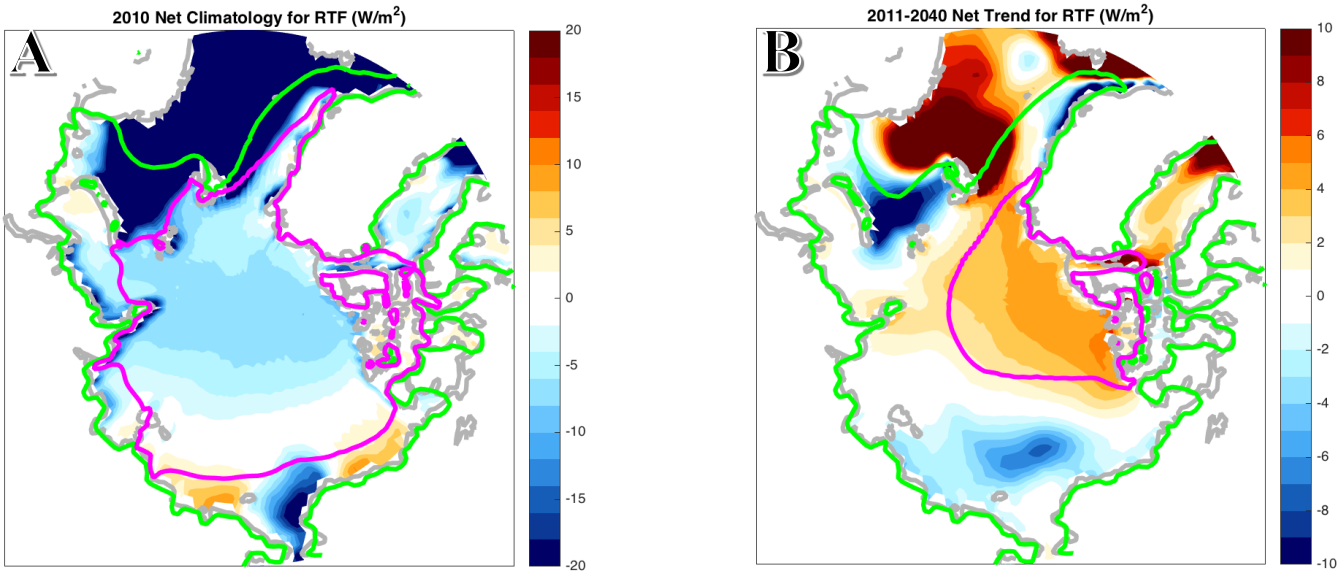

Figure 8: 2010 ensemble-mean climatology (A) and 2011-2040 trend (B) in annual net latent heat flux at the surface. Dotted (solid) green contour shows the 15% ice fraction maximum (minimum) in 2010, while the dotted (solid) pink contour shows the 15% ice fraction maximum (minimum) in 2040.

The sum of the radiative and turbulent flux trends reveals a clear energy imbalance in the Arctic with large spatial variations depending on the location's proximity to the sea ice edge. Comparing the net trends with the component fluxes makes diagnosing the central Arctic fairly simple: the loss of Arctic sea ice results in an increased amount of shortwave radiation absorption throughout the Arctic, but especially in the Central Arctic. Net longwave emissions toward space are projected to correspondingly increase, but less uniformly throughout the Arctic (e.g. the GIN Seas region experiences a net decrease in LW emissions to space) and with generally a smaller magnitude than the projected increases in net downwelling shortwave radiation.

After all four of the radiative and turbulent fluxes were tallied, some areas still show anomalous amounts of heating/cooling, with all of these regions seeming to have some sort of correlation to projected sea ice changes. The Chukchi Sea is projected to absorb somewhat more shortwave radiation ($6\frac{W}{m^2}$) in 2040 than it did in 2010 while longwave emission only increases

by about $1\frac{W}{m^2}$. This thermodynamic imbalance is overcompensated by the turbulent fluxes, as sensible and latent heat are both expected to release an additional $5.5\frac{W}{m^2}$ by 2040 leading to a net loss of energy. The Barents Sea is also expected to receive more absorbed shortwave at the surface by 2040 (~$9\frac{W}{m^2}$) with little to no change in regards to longwave release.

Seasonal Variations in the RTF Fluxes

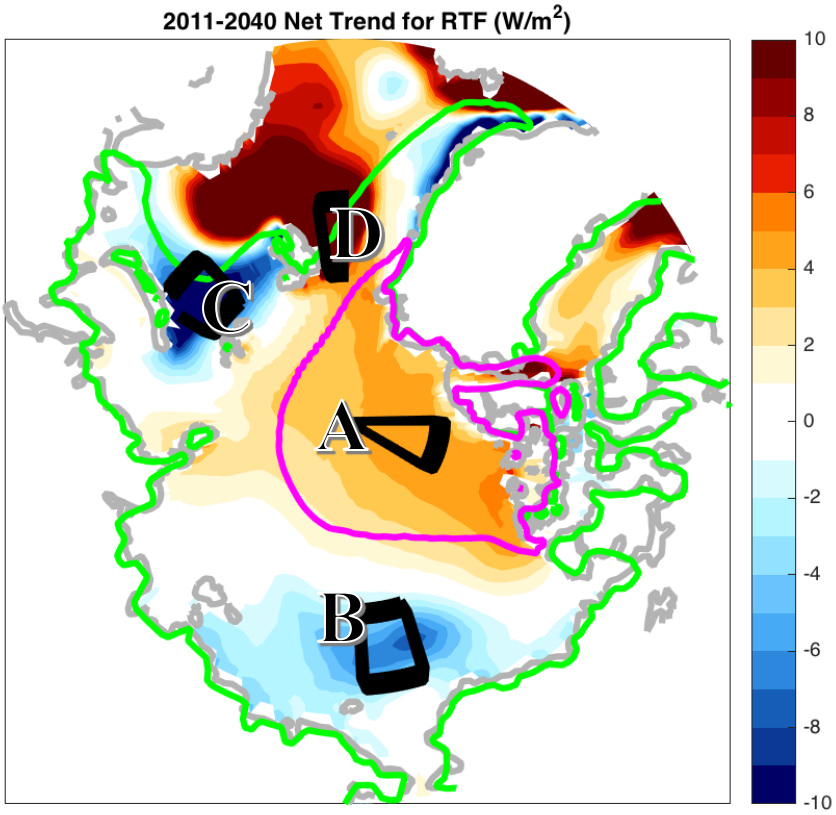

Figure 9: The net annual trend for the sum of the turbulent heat fluxes and storage (ocean heat content). Dotted (solid) green contours show the 15% ice fraction maximum (minimum) in 2010, while the dotted (solid) pink contour shows the 15% ice fraction minimum in 2040. The areas contoured in black represent the areas of particular interest in regards to their seasonal variations in the fluxes and storage terms. The area highlighted in area "A" is referred to as the Central Arctic, the area in "B" is referred to as the Chukchi Sea, area "C" is the Barents Sea, and area "D" is the GIN Seas. References to the Overall Arctic are referring to all areas north of 70°N.

Figure 9 above highlights the 4 specific regions of primary interest due to their unique variations in the surface energy budget throughout the 2011-2040 as well as their location in relation to the sea ice edge. The Central Arctic (region "A") is of note as it is still expected to be ice-covered throughout the year by 2040 thus changes to its surface heat flux are fairly straightforward: slight losses of sea ice will lead to enhanced shortwave radiation absorption. The Chukchi Sea (region "B") will undergo drastic changes to its RTF budget as the area goes from ice covered to completely ice-free by the summer of 2040. Region C, henceforth referred to as the Barents Sea, is located in a marginal ice zone during the climatology but is still located on the sea ice edge during the maximum sea ice extent in 2040. The Greenland-Iceland-Norwegian Seas (GIN Seas) (region "D") is ice-free throughout the duration of the ensemble run and is located right along the maximum sea ice extent. Lastly, there is the region that is coined as the "Overall Arctic" which encompasses all sea/ice regions from 70°N to the North Pole.

Central Arctic

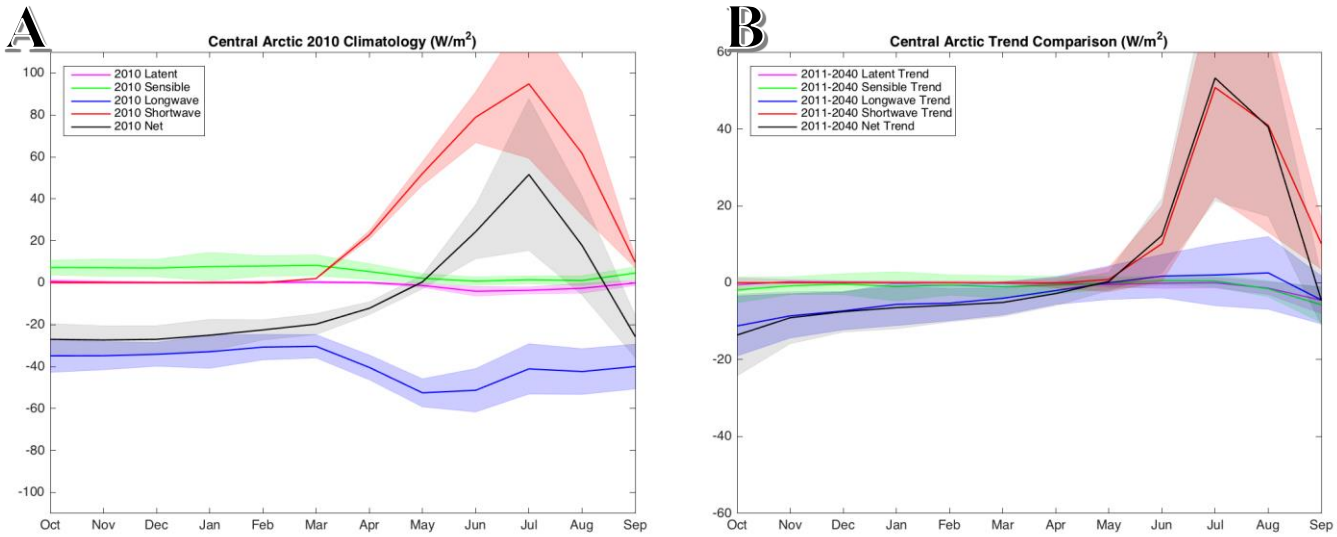

Figure 10: Seasonal variations in the turbulent and thermodynamic fluxes for the Central Arctic's 2010 Climatology (A) and 2010-2040 trend (B).

The climatology in the Central Arctic is straightforward. There is a definitive seasonal cycle, with net downward shortwave radiation absent until roughly the spring equinox, when it begins to increase at a fairly slow pace until it reaches a peak net absorption of nearly $100\frac{W}{m^2}$ in July before rapidly declining back to zero around the autumnal equinox. Shortwave absorption is offset primarily through the release of longwave radiation, which remains fairly steady ~$40\frac{W}{m^2}$ throughout the year with a slight increase in intensity during the late spring/early summer to $60\frac{W}{m^2}$. Sensible heat flux plays a minor role in the climatology of the central Arctic, inputting a relatively small amount of energy (~$5\frac{W}{m^2}$) on average into the surface. Latent heat release is nearly zero throughout the course of the year, with only a very minor contribution in the mid-summer. The sum of these turbulent terms results in a small net loss of approximately $8\frac{W}{m^2}$ for the year as the absorption of shortwave energy is not quite large enough to counter act the constantly moderate loss via longwave radiation. The largest source of ensemble variance in the Central Arctic occurs with SW radiation during summer, though roughly 95% of the range (i.e. two standard deviations) fall in a range between 59 and $130\frac{W}{m^2}$.

By 2040, the amount of shortwave absorption during the summer is expected to increase by over $50\frac{W}{m^2}$ during the mid-to-late summer months, which represents a massive (~50%) change in the overall energy budget. Longwave emissions are expected to increase by roughly $10\frac{W}{m^2}$ throughout the course of a year, but there is a decrease in the amount of longwave radiation during the late summer months. Projected changes in sensible and latent heat fluxes play only a very minor role in offsetting projected increases in shortwave absorption. Summing terms together results in a projected increase in energy added to the Central Arctic by radiative and

turbulent fluxes by about 4$\frac{W}{m^2}$. The variance in the trend of the shortwave flux during the summer with values ranging between 22-79$\frac{W}{m^2}$, is the dominant form of ensemble uncertainty. Longwave emissions exhibit a moderate amount of ensemble variability throughout the course of the year, with a standard deviation of about +/- 10 $\frac{W}{m^2}$.

Chukchi Sea

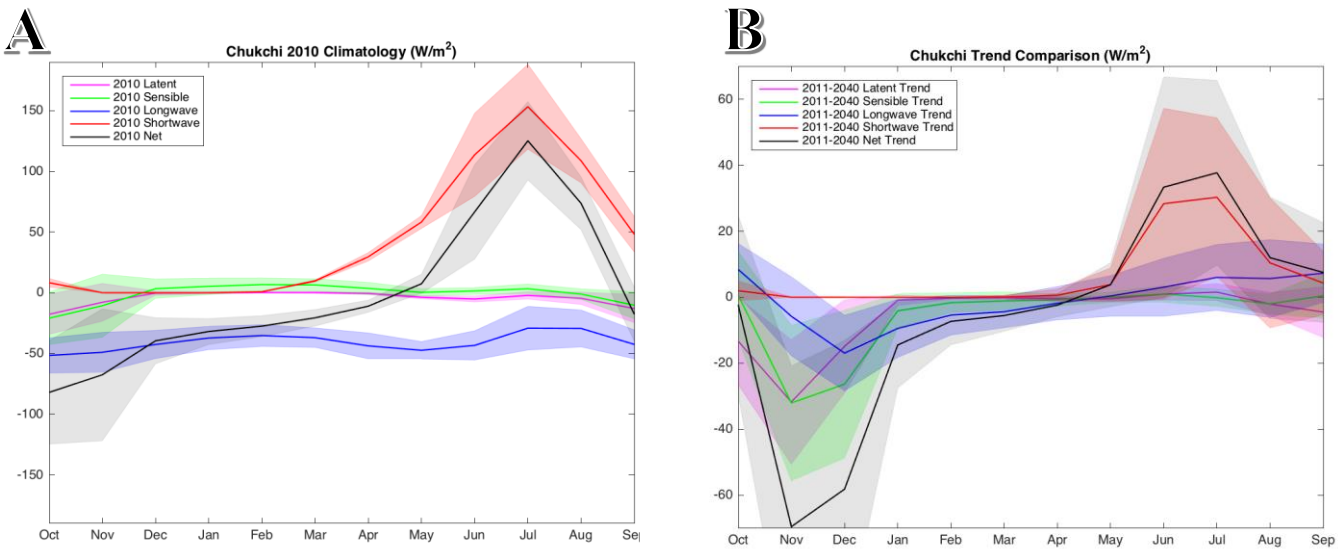

Figure 11: Seasonal variations in the turbulent and thermodynamic fluxes for the Chukchi Sea's 2010 Climatology (A) and 2010-2040 trend (B).

The Chukchi Sea has a fairly simple seasonal cycle in energy exchange that is driven mostly by seasonal changes in incoming solar radiation. Starting in late winter, net downward solar radiation begins to slowly increase from 0$\frac{W}{m^2}$ in February to its maximum value of 150$\frac{W}{m^2}$ in July before quickly declining back to 0$\frac{W}{m^2}$ in November. Latent and sensible heat fluxes play a fairly minimal role in dissipating the incoming shortwave, with an average annual latent/sensible heat release of 4.56 $\frac{W}{m^2}$ and 1.04 $\frac{W}{m^2}$, respectively. Both latent and sensible heat are strongest during the late autumn/early winter months and weakest during the spring/summertime months.

Net upward longwave radiation is the primary cooling mechanism for the Chukchi Sea region, averaging about $44\frac{W}{m^2}$ per month. Longwave release is weakest during the summer with $30\frac{W}{m^2}$ and strongest during the winter with about $50\frac{W}{m^2}$, but the seasonal cycle is relatively weak overall. The largest amount of variability across ensemble members occurs in the latent and sensible heat fluxes during winter and in shortwave flux during the summer.

All of the turbulent and thermodynamic fluxes are projected to undergo large 2010-2040 changes. Shortwave absorption is expected to increase in the summer months by ~$30\frac{W}{m^2}$, representing a 25% 20% increase in June and July, respectively. Longwave emission is expected to increase through the late-fall/early-spring and decrease the rest of the year. Latent and sensible heat are projected to account for an increasingly large role in the Chukchi energy budget, especially during the late-fall/early-winter, with latent and sensible heat releases increasing by $30\frac{W}{m^2}$ in November, marking a 300% increase in sensible heat release and a 400% increase in latent heat release. The net result in these trends is a fairly extensive amount of cooling over the course of the year, with a mean decrease of $5.44\frac{W}{m^2}$ in the amount of radiation entering the surface in by 2040. However, it is important to note that there is an extensive amount of variability in most of these fluxes, particularly in regards to latent/sensible heat in the winter and shortwave in the summer.

Barents Sea

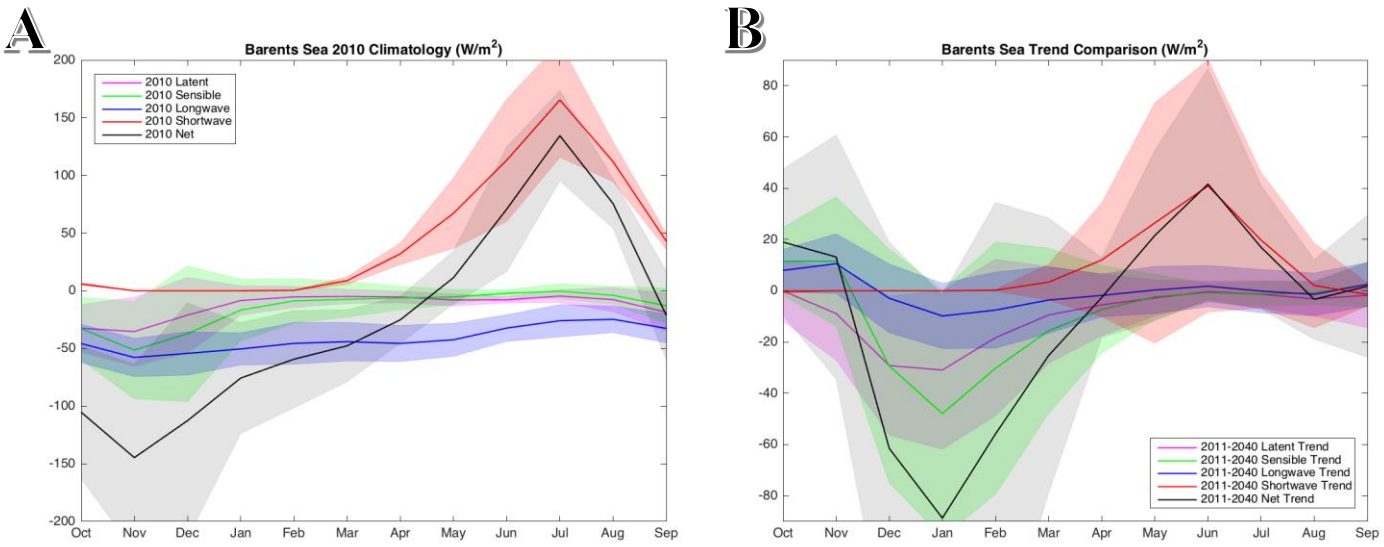

Figure 12: Seasonal variations in the turbulent and thermodynamic fluxes for the Barents' 2010 Climatology (A) and 2010-2040 trend (B).

The Barents has a fairly similar climatology profile to that of the Chukchi Sea in terms of timing/magnitudes of shortwave absorption and longwave emission, but the turbulent fluxes play a larger role in the late fall/early winter. Net downward shortwave radiation begins to slowly increase starting in March, before reaching its peak value of ~175$\frac{W}{m^2}$ in July. Net longwave emission is the primary pathway for energy loss from the surface, with an average monthly release of 50 $\frac{W}{m^2}$ throughout the year with a minor decrease during the late summer/early fall months. Latent and sensible heat also play roles in dissipating energy during the winter months, with values around 35$\frac{W}{m^2}$ throughout this time period. The net result is an average loss of roughly 25$\frac{W}{m^2}$ per month, but this stretches between a maximum net addition of about 130$\frac{W}{m^2}$ in July to a net loss of about 140$\frac{W}{m^2}$ in November.

The Barents Sea is expected to undergo a very large change in its energy budget over the course of the next 30 years. Shortwave absorption will increase during the summer, up by a

maximum of nearly 40 $\frac{W}{m^2}$ in June. Longwave absorption shows very little variation, with slight increases throughout the entire year with the exception of October and November. The largest changes are projected to occur to the latent and sensible heat fluxes. Latent heat will become an even more important dissipation term in regards to offsetting the increase of shortwave absorption, with the amount of latent heat release increasing by an average of about $9\frac{W}{m^2}$ over the course of the year, or roughly a 60% increase in magnitude relative to present values. The maximum increase in latent heat flux is projected for January at $25\frac{W}{m^2}$. Much like latent heat flux, sensible heat flux is projected to play an important role in rebalancing the Barents Sea's energy budget. The projected increase in sensible heat flux is comparable to the projected increase in latent heat flux over the Barents Sea.

Greenland-Iceland-Norwegian Seas

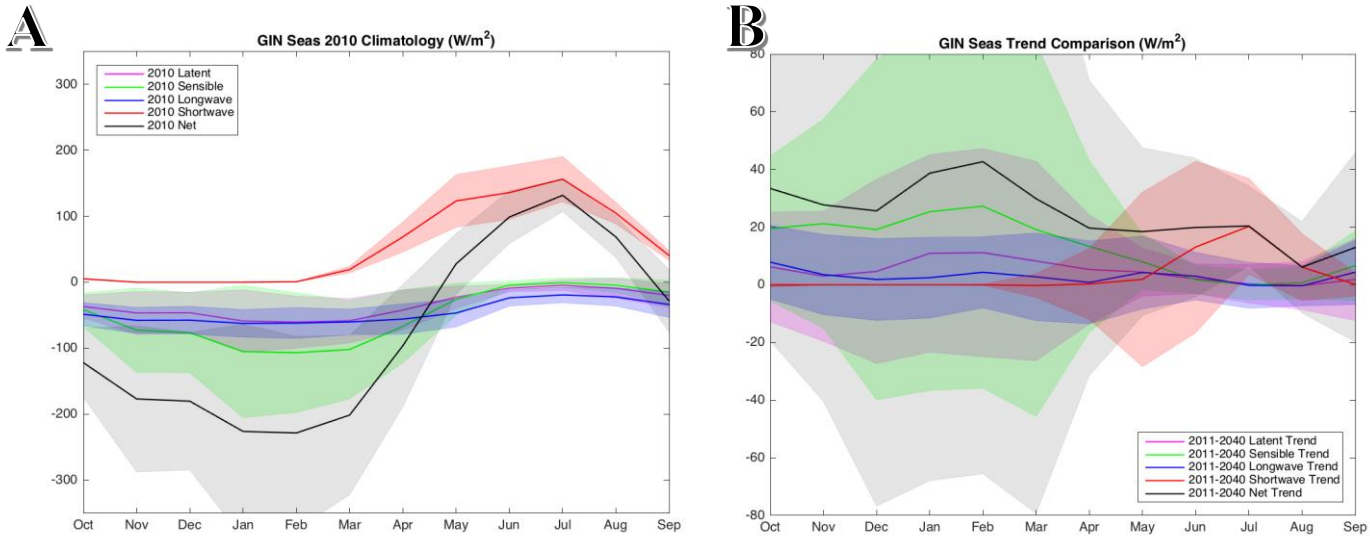

Figure 13: Seasonal variations in the turbulent and thermodynamic fluxes for the GIN Seas' 2010 Climatology (A) and 2010-2040 trend (B).

As with the regions above, net downward shortwave absorption in this region begins in March and rises slowly until reaching its peak value of $156\frac{W}{m^2}$ in June, before slowly declining

back to 0 by November. Unlike the other regions, however, latent and sensible heat release are the primary drivers for removing energy from the surface with an average monthly flux of $35\frac{W}{m^2}$ and $52\frac{W}{m^2}$, respectively. Both of these fluxes are lowest during the summer and highest during the fall and winter, with February with values of roughly $60\frac{W}{m^2}$ for latent heat and $110\frac{W}{m^2}$ for sensible heat. Longwave emissions stay fairly constant throughout the annual cycle with an average release of $44\frac{W}{m^2}$. The summation of these terms results in a large release of energy averaged over the year – roughly $80\frac{W}{m^2}$ though this imbalance is strongly seasonal.

The amount of incoming shortwave radiation, outgoing longwave radiation, and latent heat release are not expected to change much at all in the GIN Seas, at least in the annual and ensemble mean and relative to other regions. There is an increase of shortwave absorption during June and July ($13\frac{W}{m^2}$ and $20\frac{W}{m^2}$, respectively), but otherwise shortwave remains fairly unchanged. There's a slight decrease in the amount of net longwave radiation emission to space. However, there are very large changes in the amount of sensible heat release from the late-fall through the beginning of spring. During this time period, the amount of outgoing sensible heat release declines about 20% per month. With sensible heat being the primary mechanism through which energy is removed from the surface, the large declines in outgoing sensible heat are the primary reason why such substantial increases in the surface energy budget are projected in this region.

Overall Arctic

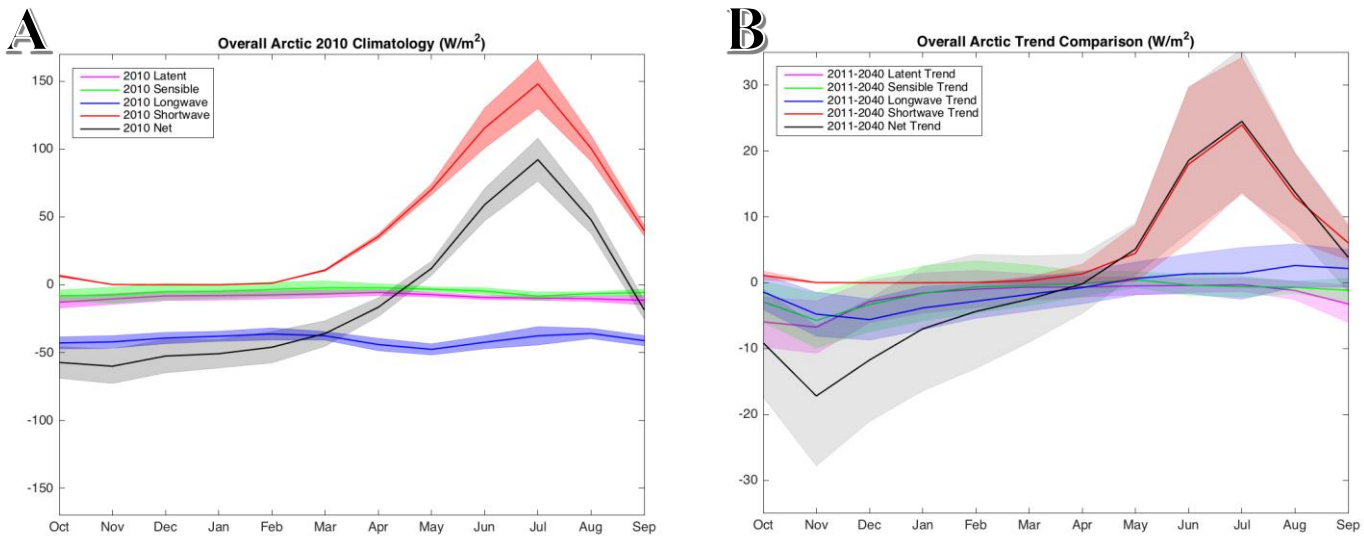

Figure 14: Seasonal variations in the turbulent and thermodynamic fluxes for the Overall Arctic's 2010 Climatology (A) and 2010-2040 trend (B).

The "Overall Arctic" as described above refers to the Arctic Ocean poleward of 70° North. As with the other cases, shortwave radiation begins to enter the system starting in March before reaching its peak of 148$\frac{W}{m^2}$ in July. Latent and sensible heat play minor roles in modifying the net radiative heating, but there's very little variation in the magnitude of these terms throughout the seasonal cycle, averaging only about 9$\frac{W}{m^2}$ and 5$\frac{W}{m^2}$. The dominant cooling term is longwave emission, which also shows very little variation month-to-month with an average of 40$\frac{W}{m^2}$. Compared to the above regions, there is much less variation in the terms, due mostly to the large compensating spatial average with only shortwave showing a large spread of about 10$\frac{W}{m^2}$ during the summertime months.

The projected 2011-2040 changes in the turbulent and thermodynamic heat fluxes will be important, but especially regionally and perhaps not as much from a pan-Arctic perspective. Shortwave absorption is expected to increase by 15-25$\frac{W}{m^2}$ during the summer. Latent heat is

expected to increase by $2\frac{W}{m^2}$ while sensible heat is going to increase by $1.4\frac{W}{m^2}$. Longwave emissions increase during the winter and decrease during the summer, but only net out to about $1\frac{W}{m^2}$ of additional release. There is a large amount of variation throughout the annual cycle, particularly during the summer and early winter.

Energy Pathways

Much of the Arctic is experiencing radiative and turbulent imbalances, so in order to conserve energy there must be storage or transport occurring. In the case of the surface, losses or gains of energy in regards to RTF flux differences must be compensated by either oceanic transport or storage. The storage in this region can be determined by evaluating changes in the oceanic heat content in the ocean, which in this case is estimated to be the upper 100 meters of the ocean. Oceanic transport, while not directly calculated, can be estimated by the difference between ocean heat content and the net change in the RTF fluxes. Furthermore, the atmospheric energy budget is also studied to evaluate how these energy imbalances in the surface are realized in the atmosphere. The difference between radiative terms between the top of the atmosphere and the surface combined with upward turbulent fluxes can be used to calculate the combined amount of atmospheric energy storage and transport in any given region. While these two terms cannot be separated due to computational constraints, other variables such as sea level pressure and temperature can deduce the magnitude and role of atmospheric transport/storage in a given location.

Ocean Heat Content

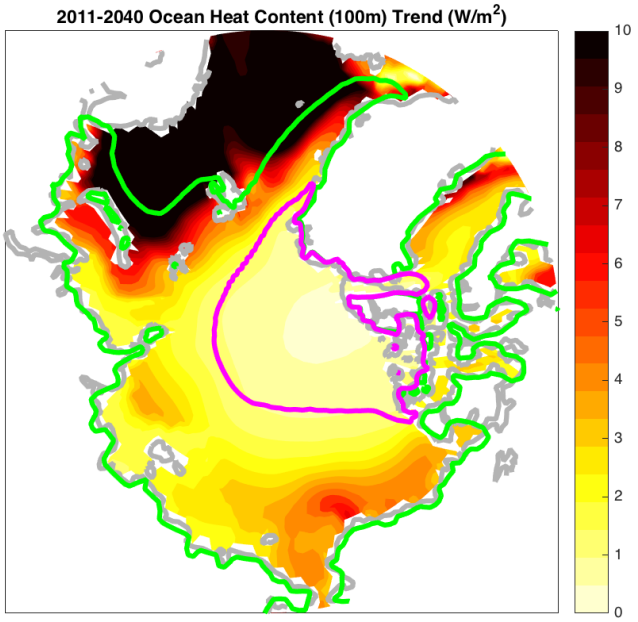

Figure 15: 2011-2040 trends in ocean heat content for the uppermost 100 meters in the ocean.

The trends in ocean heat content (figure 15) are very similar to what was seen in regards to sea ice loss: ocean heat content trends are greatest in ice-free and marginal ice zones, with the largest values occurring in the Barents/GIN Seas, and smallest in the areas with high sea ice concentration. This plot, in conjunction with the net RTF plot, can help provide insight into which areas are experiencing larger amounts of oceanic transport.

Atmospheric Storage and Transport

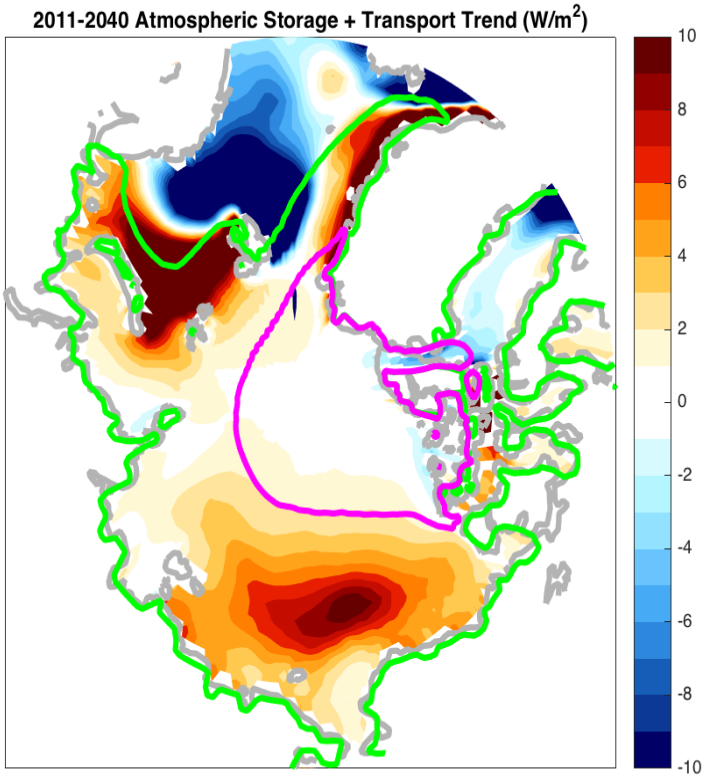

Figure 16: 2011-2040 trends in the atmospheric storage and transport term.

The atmospheric storage and transport spatial variability bears a strong resemblance to the net RTF fluxes at the surface, with the main difference being a switching of signs (figure 16) which is to be expected. Areas that are losing energy at the surface (Chukchi and Barents Seas) to the atmosphere are generally experiencing increases to their atmospheric storage/transport. This is not universal as the inclusion of the TOA fluxes has an impact on the magnitude in some regions. For example, in the Chukchi Sea, more energy is being stored/transported in the atmosphere than there was being released from the surface. Also of note, the differences between the TOA and the surface account for the warming at the surface in the Central Arctic, as there is no storage or transport in this region whatsoever. This plot is imperative in understanding the atmospheric energy budget and the strength of atmospheric storage/transport.

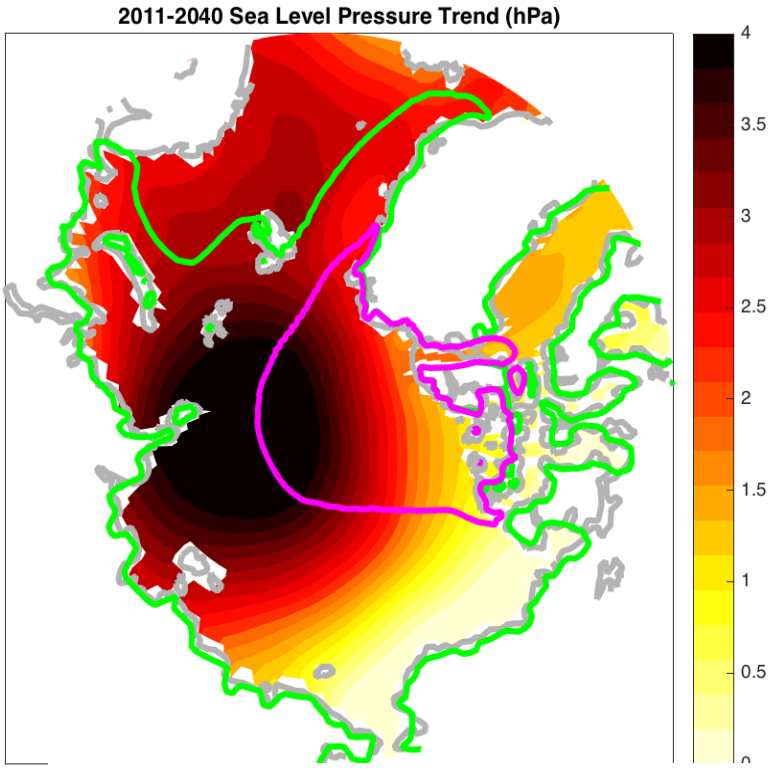

Figure 17: 2011-2040 trends in sea level pressure.

Sea level pressure trends show a fairly strong change of about 4 hPa in sea level in the central portion of the Arctic (figure 17). This pattern is interesting in that there appears to be no correlation between sea pressure trends and sea ice concentration. This pressure perturbation could have large impacts on both sea ice extent and surface turbulent fluxes. A high pressure system could act to remove sea ice from the Barents Sea and push it against Iceland or Greenland through atmospheric circulations. Furthermore, this high pressure could have strong impacts on the surface turbulent fluxes, as Deser et. al (2000) have shown that off-ice flows allows for massive turbulent heat exchange between the cold, dry atmosphere and the (relatively) warm ocean. This sea level trend will be discussed in further detail in the discussion portion.

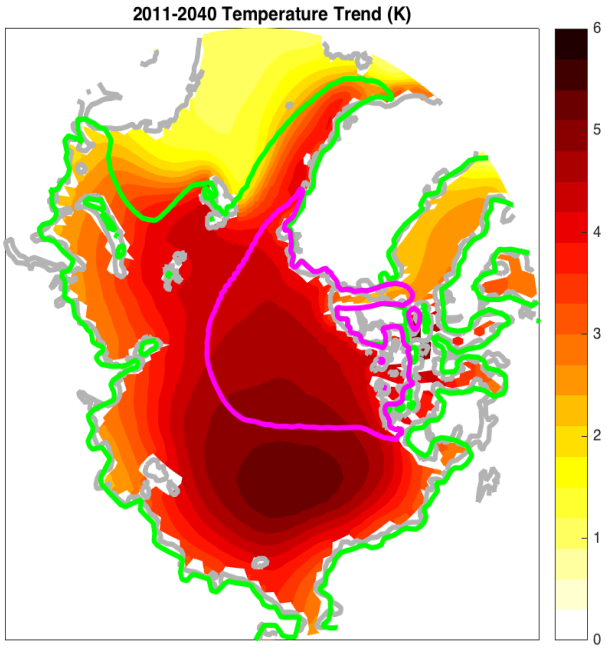

Figure 18: 2011-2040 trends in surface temperature.

Figure 18, which shows 2011-2040 surface temperature trends, reveals widespread warming throughout the Arctic with the largest values occurring in areas that were previously dominated by sea ice coverage. The Chukchi Sea region experiences the largest increase in temperatures of ~5K, while the often chaotic GIN and Barents Seas only see an increase of about 1K and 2.5K, respectively. It is interesting to note, however, that while there is a distinct difference between temperature changes in sea ice covered areas versus the open ocean, there is really no correlation between temperature trend and sea ice concentration. For example, there is not anomalous warming in the Central Arctic where it is still heavily concentrated with sea ice.

Chapter 4. Discussion

Sea ice coverage plays the dominant role in determining the Arctic surface energy budget on both a spatial and seasonal scale: the more sea ice decline or variability there is in the particular region, the more complex and chaotic the system becomes. Areas that are still ice-

covered year-round by year 2040 are seeing fairly predictable trends while areas that are marginally ice-covered or completely-ice free by 2040 are experiencing highly volatile changes. As such, examining the Arctic on a regional basis provides the most insight into why the fluxes are changing.

Piecing it all Together

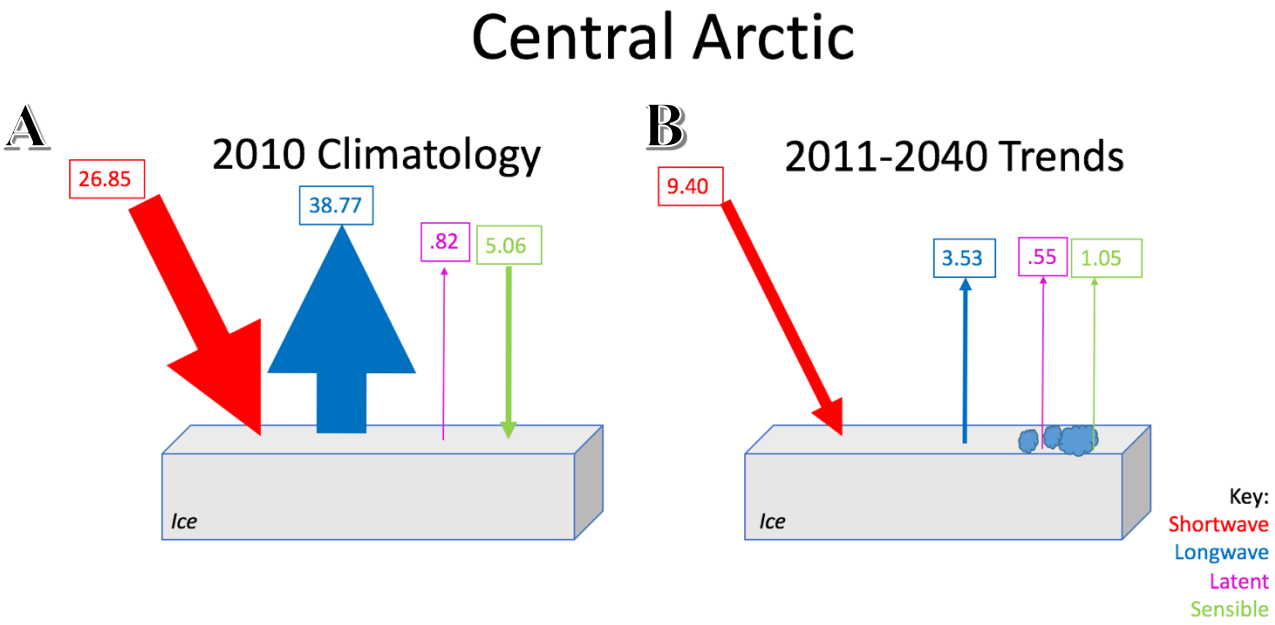

Figure 19: The 2010 annual mean climatology (A) and 2011-2040 mean net trends (B) for the various RTF fluxes in the Central Arctic. The width of the arrows is directly correlated to the size of the flux.

The Central Arctic has the most simplistic energy budget to analyze out of the four anomalous regions. In the climatology, the central arctic is completely ice covered, thus the amount of shortwave absorption is fairly small (figure 19a). Energy loss is almost entirely though longwave release with only an incredibly small amount due to latent heat. Sensible heat is transferred from the atmosphere to warm sea ice, but otherwise turbulent fluxes do not play a large role in the energy budget as the thick sea ice prevents atmospheric-oceanic transfers of energy. By 2040, declines in both ice thickness and sea ice coverage allow for higher shortwave

absorption (figure 19b). Longwave emission, latent heat, and sensible heat all act to remove this excess energy but their small sizes area not large enough to offset this excess energy, resulting in a net increase in energy absorbed by the surface. Atmospheric transport and storage appear to play a minor role in this region (figure 16) as the small amount of energy that is being stored (as implied by the small increase in temperatures in figure 18) must be advected out of the region. This means that the small increase in the surface RTF fluxes is primarily being used to warm the surface ocean waters as evident by the increased ocean heat content.

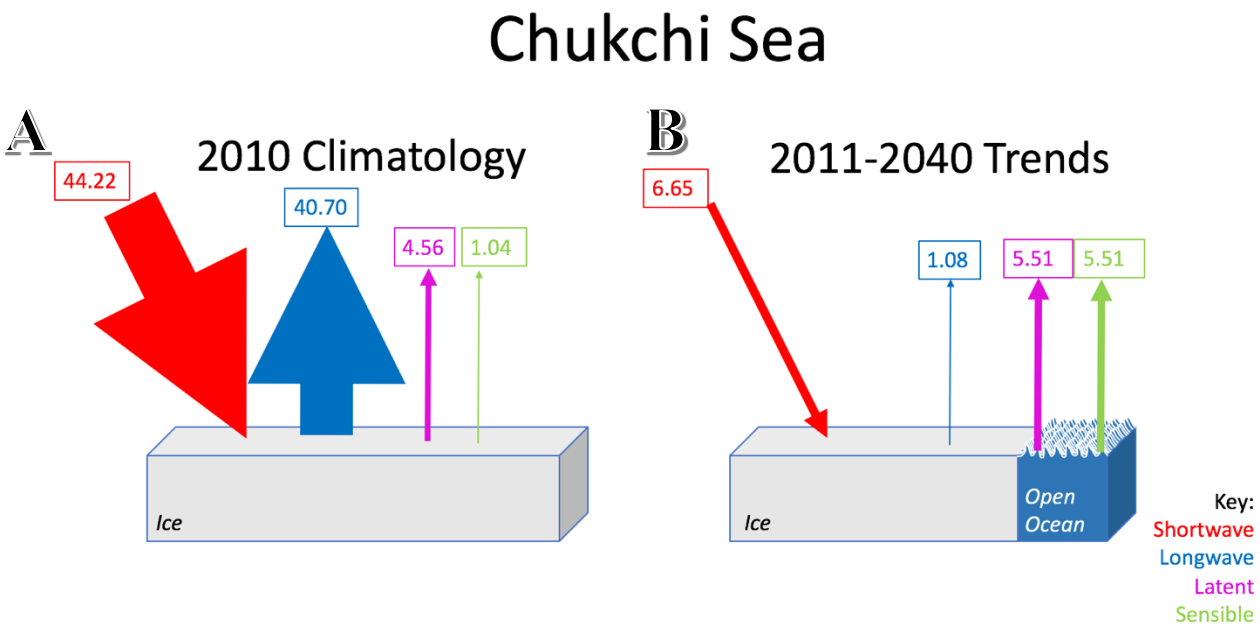

Figure 20: The 2010 annual mean climatology (A) and 2011-2040 mean net trends (B) for the various RTF fluxes in the Chukchi Sea. The width of the arrows is directly correlated to the size of the flux.

The climatology for the Chukchi Sea is very similar to that of the central Arctic, however the lower sea ice thicknesses and concentrations result in stronger turbulent heat fluxes from the ocean to the atmosphere, particularly in regards to latent heat release (figure 20a). During the 2011-2040 timeframe of interest, the Chukchi Sea transitions from being nearly ice covered year-round to a marginal ice zone. This decline in ice coverage results in more shortwave absorption

due to the low albedo of open water as well as increases in upward turbulent fluxes due to the large gradients in both temperature and moisture between the atmosphere and the ocean (figure 20b). Longwave emissions do not vary much at all in this region between 2011 and 2040. There is also an increase in the amount of energy being stored in the surface ocean. For the Chukchi Sea to be in energy balance at the surface, the loss of energy via RTF fluxes and the increased OHC implies that oceanic transport into this region must be substantial. In regards to the atmosphere, the energy being released from the surface appears to be primarily stored in the atmosphere due to the large increase in temperature as seen in figure 18. However, since atmospheric storage and transport cannot be separated, atmospheric transport cannot be ruled out.

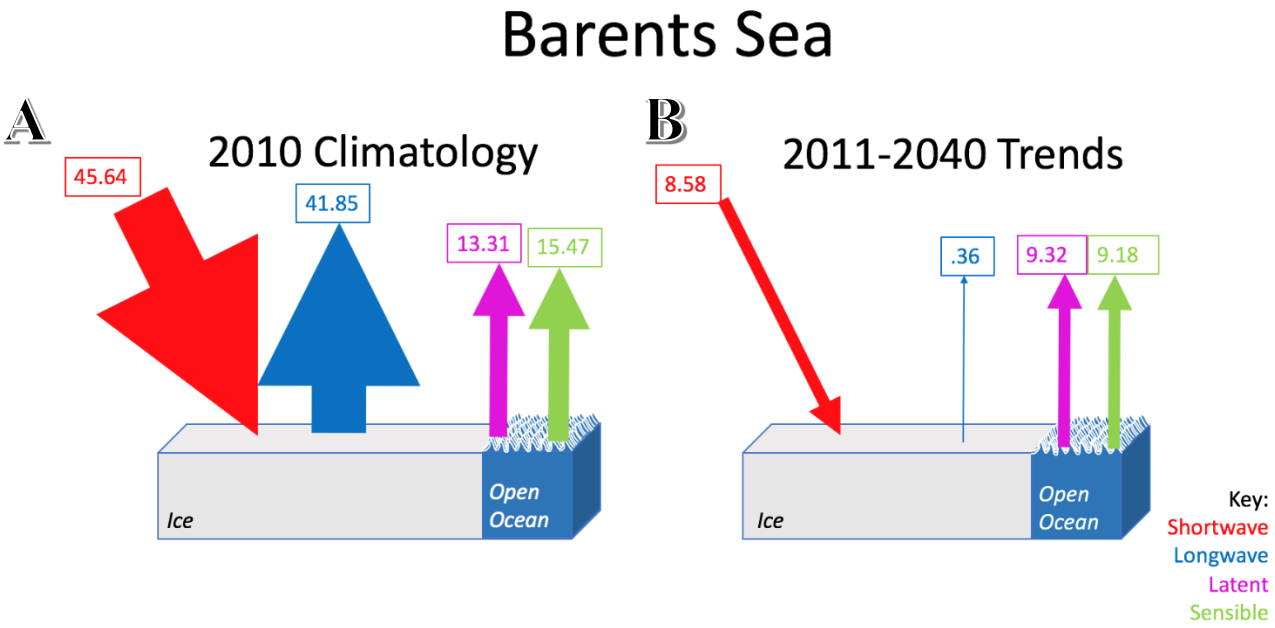

Figure 21: The 2010 annual mean climatology (A) and 2011-2040 mean net trends (B) for the various RTF fluxes in the Barents Sea. The width of the arrows is directly correlated to the size of the flux.

The Barents Sea is already located in a marginal ice zone in the climatology, which is why this region is experiencing greater shortwave absorption and larger outgoing turbulent heat fluxes than the Chukchi Sea and Central Arctic (figure 21a). Between 2011 and 2040, ice

thickness and extent continue to decline in this region, further exposing ocean to the atmosphere and allowing for greater turbulent heat exchange and shortwave absorption (figure 21b). Much like the Chukchi Sea, decreases in the surface RTF fluxes combined with an increase in ocean heat content means that oceanic transport must increase substantially to maintain energy balance at the surface. The energy lost in the surface moves into the atmosphere, and while storage may be important it appears that atmospheric transport is the primary driver in maintaining the energy balance in the atmosphere. This will be discussed in further detail in the GIN Seas section.

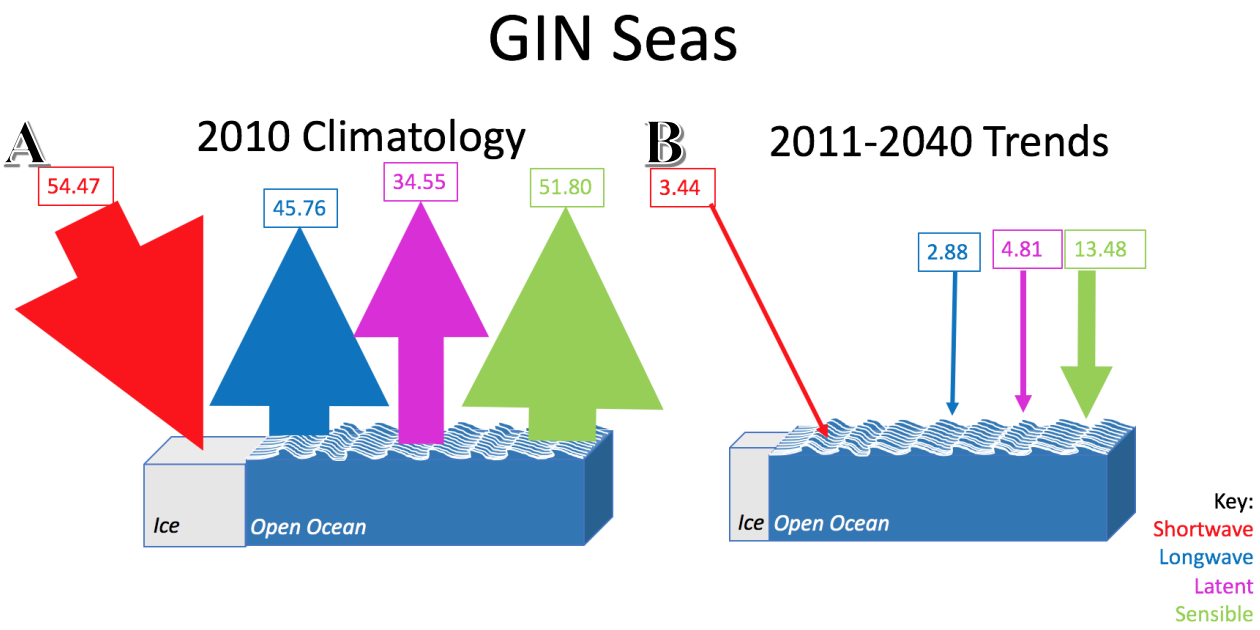

Figure 22: The 2010 annual mean climatology (A) and 2011-2040 mean net trends (B) for the various RTF fluxes in the GIN Seas. The width of the arrows is directly correlated to the size of the flux.

The GIN Seas is being strongly influenced by oceanic transport into the region, as seen by the massive amount of energy being lost in this region in the climatology (figure 22a). However, by 2040, the amount of energy being released in this area declines quite dramatically, as its strongest turbulent flux (sensible heat) declines by 26% (figure 22b). Ocean heat content is

increasing in this area, as would be expected due to the increase in shortwave absorption as well as the large declines in outgoing turbulent heat fluxes. The atmospheric storage and transport plot is also showing massive changes in this region. Modest increases in surface temperature show that atmospheric storage is likely, but not large. This means that atmospheric transport must be playing a large role in this area, an idea that is corroborated by the changes in the sea level pressure (figure 23).

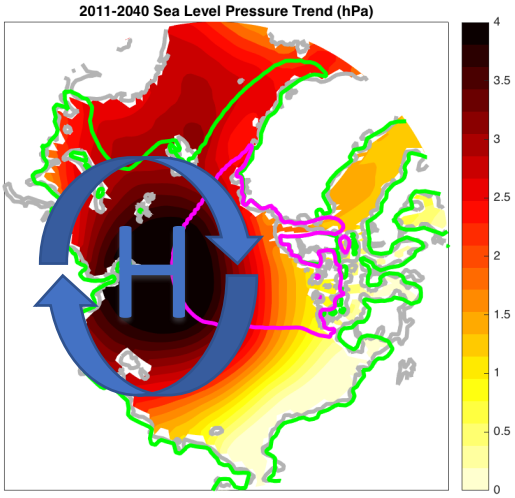

Figure 23: The 2011-2040 sea level pressure trends with overlying high pressure graphic. This alteration in flow may explain the large changes in the Barents and GIN Seas.

Changes in sea level pressure form a high pressure system in the Arctic, which causes anti-cyclonic flow (figure 23). Looking at the Barents Sea and GIN Seas regions, this results in off-ice flow that strikes the Barents Sea first before reaching the GIN Seas. As the Barents Sea is now the area of first contact between cold, dry air and the warm ocean, it is now able to dump much more energy in the form of turbulent heat flux. As this air is now warmer and more heavily concentrated in terms of water vapor, the temperature and moisture gradients between the atmosphere and the GIN Seas is now smaller. This results in the GIN Seas releasing a smaller

amount of energy from the ocean to the atmosphere than it had in the past. This explains why there is such a strong dipole signature in this region: the change in atmospheric circulations (and subsequent transport) greatly impacts the surface RTF fluxes. This relationship between off-ice flows and turbulent heat exchange is very similar to that described by Deser et. al, 2000.

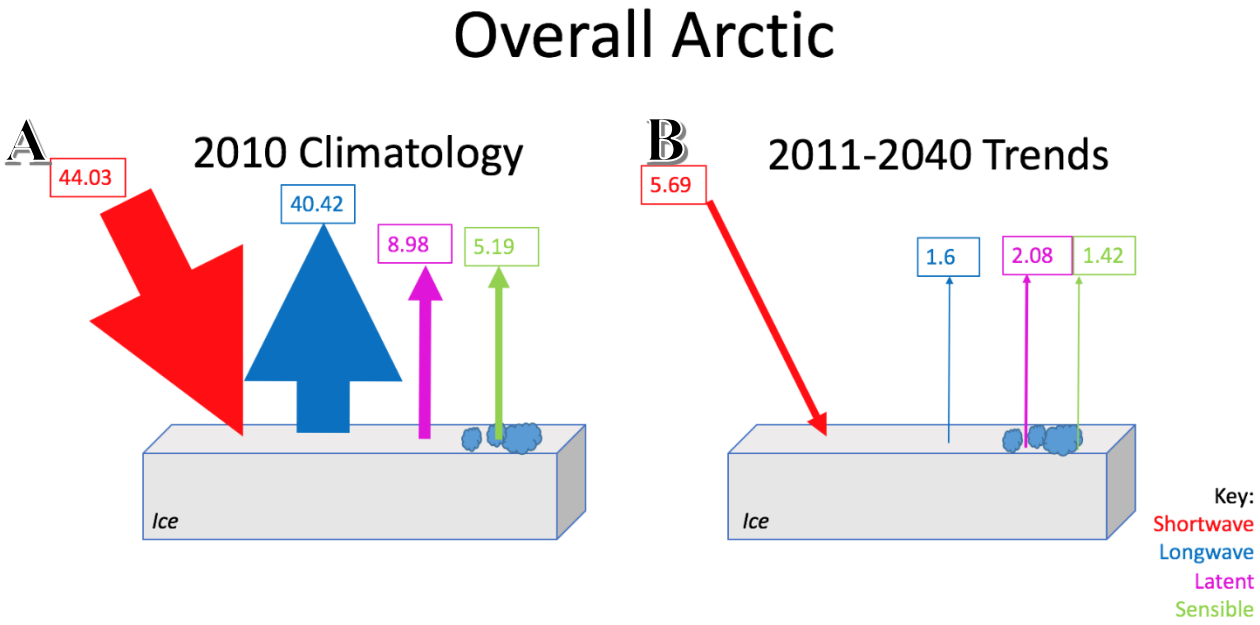

Figure 24: The 2010 annual mean climatology (A) and 2011-2040 mean net trends (B) for the various RTF fluxes in the Overall Arctic. The width of the arrows is directly correlated to the size of the flux.

The Arctic climatology shows that shortwave absorption is primarily offset by longwave emission, with some contributions from latent and sensible heat (figure 24a). There is a clear energy imbalance in the Arctic climatology as the energy being released from the surface greatly exceeds the amount entering, as would be expected in the higher latitudes. By 2040, the changes are fairly basic, wherein decreased sea ice extent results in more shortwave absorption with minor increases in outgoing longwave as well as turbulent and sensible heat release (figure 24b). The sum of these components show that the Arctic as a whole is only absorbing about $.5\frac{W}{m^2}$ more

in 2040 than it had in 2010. However, explaining these changes is simply not possible due to large spatial coverage and heterogeneity of the fluxes throughout the domain.

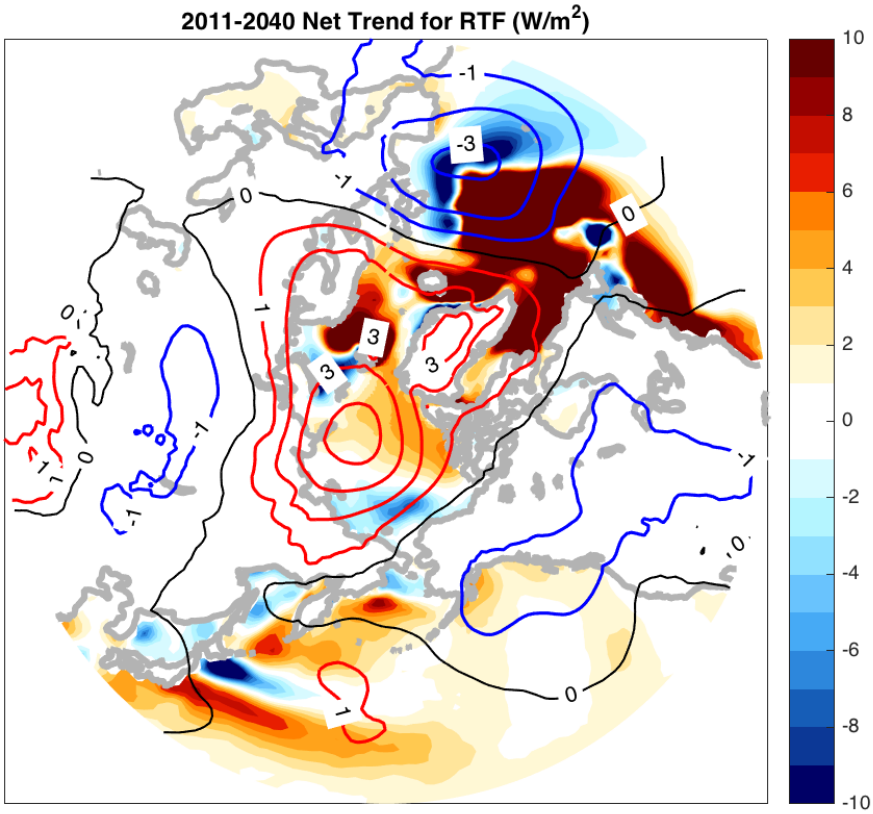

Figure 25: The 2011-2040 net surface RTF trend with overlying 2011-2040 sea level pressure trends.

Figure 25 shows us that there is still much to be learned in regards to the Arctic energy budget and atmospheric circulations. Figure 56 shows the net of the 2011-2040 trends in the surface RTF fluxes with the 2011-2040 trends in sea level pressure contoured above it. Analyzing the differences in sea level pressure down to the midlatitudes reveals an interesting wave train pattern emanating from the northern Atlantic and proceeding through northern Europe. This curved pattern in sea level pressure disturbances is typically tropically forced and does not appear to be driven by changes to sea ice extent (Wettstein and Deser, 2014; Ding et. al, 2014). This further highlights the fact that utilizing fully-coupled models is truly necessary to

create dynamically and thermodynamically realistic projections as this pattern would be missing in atmosphere-only simulations.

Chapter 5. Conclusions & Future Work

A one-dimensional view of the Arctic using CESM1-CAM5 reveals drastic changes to the Arctic surface energy budget on both a spatial and seasonal basis. Treating the Arctic as a singular system does not provide an accurate portrayal as to what is actually occurring in this region as there are substantial variations in the Arctic surface energy budget that may have widespread implications in regards to both the transport and storage of energy. However, it is clear that the amount/location of sea ice does provide structure to these variations. In the Central Arctic, the high amount of sea ice results in an energy budget that is fairly simplistic in nature, whereby increased shortwave radiation is simply being absorbed by the ocean with some minor transport via ocean currents. As the amount of sea ice becomes more variable, so do the component fluxes. In the Chukchi Sea for example, the decrease in sea ice throughout the year not only leads to more shortwave absorption but significantly more energy release from the ocean to the atmosphere. This energy loss of energy at the surface indicates that ocean currents must be supplying energy to offset this energy loss while at the same time the atmosphere is absorbing more energy as indicated by the increased temperatures and storage/transport term. The Barents and GIN Seas appear to be most heavily impacted by alterations in atmospheric circulations as the trends towards higher pressure in the Arctic results in more off-ice flow moving over the now-exposed open ocean in the Barents Sea. This allows for a massive exchange of turbulent energy between the ocean and the atmosphere in the Barents Sea, but a decrease in the amount of turbulent heat loss in the GIN Seas as the air is now warmer and

contains more water vapor. In summary, the Arctic is very complex and cannot be looked upon as a single system, there is large heterogeneity in the manner through which the Arctic surface energy budget is currently presented and expected to change.

In regards to carrying on this project, there are a number of ways this could be expanded. The most logical progression would be to explicitly solve for atmospheric storage by integrating throughout the atmospheric column as well as developing ocean heat content estimates based off realistic and dynamic mixed layer profiles. By explicitly solving for both atmospheric and oceanic content the full budgets for both the surface and the atmosphere can be solved and analyzed quantitatively (assuming the conservation of energy). Future work could also include cross-checking findings in this paper with established observational and reanalysis data to analyze how well the model is replicating current ice conditions. While previous studies have shown this model to successfully recreate a variety of sea ice and atmospheric conditions, ensuring the model still holds up to more recent observations would also help lend credence to the model's projections. Another natural avenue through which this work could be continued would be to evaluate trends and establish correlations between the differences in the Arctic surface energy budget detailed above and temperature/precipitation anomalies in the Arctic and subpolar regions.

This study highlights the fact that the Arctic is an incredibly complex system that must be continuously reevaluated as our modeling and computing capabilities continue to grow. Fully-coupled models are the lens through which this area should be studied: while utilizing prescribed components may be beneficial for diagnosing certain dynamic and thermodynamic traits, only fully-coupled modeling will establish realistic and accurate results.

Bibliography

Alexander, M.A., Bhatt, U.S., Walsh, J.E., Timlin, M.S., Miller, J.S. and Scott, J.D., 2004. The atmospheric response to realistic Arctic sea ice anomalies in an AGCM during winter. *Journal of climate, 17*(5), pp.890-905.

Barnes, E.A., 2013. Revisiting the evidence linking Arctic amplification to extreme weather in midlatitudes. *Geophysical Research Letters*, *40*(17), pp.4734-4739.

Blackport, R. and Kushner, P.J., 2016. The transient and equilibrium climate response to rapid summertime sea ice loss in CCSM4. *Journal of Climate*, *29*(2), pp.401-417.

Deser, C., Walsh, J.E. and Timlin, M.S., 2000. Arctic sea ice variability in the context of recent atmospheric circulation trends. *Journal of Climate*, *13*(3), pp.617-633.

Deser, C., Tomas, R., Alexander, M. and Lawrence, D., 2010. The seasonal atmospheric response to projected Arctic sea ice loss in the late twenty-first century. *Journal of Climate*, *23*(2), pp.333-351.

Deser, C., Tomas, R.A. and Sun, L., 2015. The role of ocean–atmosphere coupling in the zonal-mean atmospheric response to Arctic sea ice loss. *Journal of Climate*, *28*(6), pp.2168-2186.

Ding, Q., Wallace, J.M., Battisti, D.S., Steig, E.J., Gallant, A.J., Kim, H.J. and Geng, L., 2014. Tropical forcing of the recent rapid Arctic warming in northeastern Canada and Greenland. *Nature*, *509*(7499), pp. 209-212.

Ebert, E.E. and Curry, J.A., 1993. An intermediate one-dimensional thermodynamic sea ice model for investigating ice-atmosphere interactions. *Journal of Geophysical Research: Oceans*, *98*(C6), pp.10085-10109.

Francis, J.A. and Vavrus, S.J., 2012. Evidence linking Arctic amplification to extreme weather in mid-latitudes. *Geophysical Research Letters*, *39*(6).

Jahn, A., Sterling, K., Holland, M.M., Kay, J.E., Maslanik, J.A., Bitz, C.M., Bailey, D.A., Stroeve, J., Hunke, E.C., Lipscomb, W.H. and Pollak, D.A., 2012. Late-twentieth-century simulation of Arctic sea ice and ocean properties in the CCSM4. *Journal of Climate*, *25*(5), pp.1431-1452.

Kay, J.E., Hillman, B.R., Klein, S.A., Zhang, Y., Medeiros, B., Pincus, R., Gettelman, A., Eaton, B., Boyle, J., Marchand, R. and Ackerman, T.P., 2012. Exposing global cloud biases in the Community Atmosphere Model (CAM) using satellite observations and their corresponding instrument simulators. *Journal of Climate*, *25*(15), pp.5190-5207.

Krikken, F. and Hazeleger, W., 2015. Arctic energy budget in relation to sea ice variability on monthly-to-annual time scales. *Journal of Climate*, *28*(16), pp.6335-6350.

Liu, J., Curry, J.A., Wang, H., Song, M. and Horton, R.M., 2012. Impact of declining Arctic sea ice on winter snowfall. *Proceedings of the National Academy of Sciences*, *109*(11), pp.4074-4079.

Magnusdottir, G., Deser, C. and Saravanan, R., 2004. The effects of North Atlantic SST and sea ice anomalies on the winter circulation in CCM3. Part I: Main features and storm track characteristics of the response. *Journal of Climate*, *17*(5), pp.857-876.

Meehl, G.A., Washington, W.M., Arblaster, J.M., Hu, A., Teng, H., Kay, J.E., Gettelman, A., Lawrence, D.M., Sanderson, B.M. and Strand, W.G., 2013. Climate change projections in CESM1 (CAM5) compared to CCSM4. *Journal of Climate*, *26*(17), pp.6287-6308.

Nakamura, N. and Oort, A.H., 1988. Atmospheric heat budgets of the polar regions. *Journal of Geophysical Research: Atmospheres*, *93*(D8), pp.9510-9524.

Neale, R.B., Chen, C.C., Gettelman, A., Lauritzen, P.H., Park, S., Williamson, D.L., Conley, A.J., Garcia, R., Kinnison, D., Lamarque, J.F. and Marsh, D., 2010. Description of the NCAR community atmosphere model (CAM 5.0). *NCAR Tech. Note NCAR/TN-486+ STR*.

Oort, A.H., 1974. Year-to-year variations in the energy balance of the arctic atmosphere. *Journal of Geophysical Research*, *79*(9), pp.1253-1260.

Overland, J.E. and Pease, C.H., 1982. Cyclone climatology of the Bering Sea and its relation to sea ice extent. *Monthly Weather Review*, *110*(1), pp.5-13.

Peralta-Ferriz, C. and Woodgate, R.A., 2015. Seasonal and interannual variability of pan-Arctic surface mixed layer properties from 1979 to 2012 from hydrographic data, and the dominance of stratification for multiyear mixed layer depth shoaling. *Progress in Oceanography*, *134*, pp. 19-53.

Peings, Y. and Magnusdottir, G., 2014. Response of the wintertime Northern Hemisphere atmospheric circulation to current and projected Arctic sea ice decline: A numerical study with CAM5. *Journal of Climate*, *27*(1), pp.244-264.

Seierstad, I.A. and Bader, J., 2009. Impact of a projected future Arctic sea ice reduction on extratropical storminess and the NAO. *Climate dynamics*, *33*(7-8), pp.937-943.

Semmler, T., McGrath, R. and Wang, S., 2012. The impact of Arctic sea ice on the Arctic energy budget and on the climate of the Northern mid-latitudes. *Climate Dynamics*, *39*(11), pp.2675-2694.

Serreze, M.C., Barrett, A.P., Slater, A.G., Steele, M., Zhang, J. and Trenberth, K.E., 2007. The large-scale energy budget of the Arctic. *Journal of Geophysical Research: Atmospheres*, *112*(D11).

Sorokina, S.A., Li, C., Wettstein, J.J. and Kvamstø, N.G., 2016. Observed atmospheric coupling between Barents Sea ice and the warm-Arctic cold-Siberian anomaly pattern. *Journal of Climate*, *29*(2), pp.495-511.

Sorteberg, A., Kattsov, V., Walsh, J.E. and Pavlova, T., 2007. The Arctic surface energy budget as simulated with the IPCC AR4 AOGCMs. *Climate Dynamics*, *29*(2-3), pp.131-156.

Stroeve, J., Holland, M.M., Meieer, W., Scambos, T. and Serreze, M. 2007. Arctic sea ice decline: Faster than forecast. *Geophysical research letters, 34*(9).

Wettstein, J.J. and Deser, C., 2014. Internal variability in projections of twenty-first-century Arctic sea ice loss: Role of the large-scale atmospheric circulation. *Journal of Climate, 27*(2), pp. 527-550.

Appendices

Regional Turbulent and Thermodynamic Climatology/Trend Tables

Chukchi Sea

Chukchi Turbulent and Thermodynamic Climatology (W/m^2)					
	Latent Heat	**Sensible Heat**	**Longwave**	**Shortwave**	**Net TTF Fluxes**
January	0.04	5.31	-37.28	0.00	-31.93
February	0.20	6.73	-35.27	0.84	-27.50
March	0.17	6.45	-37.00	9.74	-20.64
April	-0.56	3.60	-43.77	29.65	-11.07
May	-3.75	0.32	-47.40	58.24	7.42
June	-5.16	1.50	-43.35	113.67	66.66
July	-2.20	3.30	-29.17	153.26	125.18
August	-4.58	-1.09	-29.40	108.71	73.63
September	-13.01	-10.27	-42.51	48.17	-17.62
October	-17.73	-20.96	-51.65	8.25	-82.08
November	-7.86	-10.70	-49.06	0.05	-67.57
December	-0.33	3.36	-42.61	0.00	-39.58
Net Annual	-54.76	-12.45	-488.46	530.58	-25.09
Mean Monthly	-4.56	-1.04	-40.70	44.22	-2.09

Chukchi Turbulent and Thermodynamic Trends (W/m^2)					
	Latent Heat	**Sensible Heat**	**Longwave**	**Shortwave**	**Net TTF Fluxes**
January	-0.91	-4.12	-9.44	0.00	-14.47
February	-0.25	-1.64	-5.40	-0.01	-7.30
March	-0.12	-1.12	-4.40	0.09	-5.54
April	-0.39	-0.78	-1.82	0.60	-2.39
May	-0.46	0.02	0.40	3.83	3.78
June	0.97	0.99	3.03	28.34	33.33
July	1.56	-0.13	6.00	30.29	37.71
August	-2.07	-2.02	5.66	10.41	11.98
September	-4.51	0.46	7.28	4.28	7.51
October	-13.30	0.63	8.43	1.98	-2.25
November	-31.73	-32.03	-5.76	0.01	-69.51
December	-14.88	-26.34	-16.93	0.00	-58.15
Net Annual	-66.07	-66.08	-12.97	79.83	-65.30
Mean Monthly	-5.51	-5.51	-1.08	6.65	-5.44

Central Arctic

Central Arctic Turbulent and Thermodynamic Climatology (W/m^2)					
	Latent Heat	Sensible Heat	Longwave	Shortwave	Net TTF Fluxes
January	0.15	7.72	-32.89	0.00	-25.02
February	0.23	7.98	-30.70	0.00	-22.49
March	0.26	8.31	-30.31	2.01	-19.74
April	0.06	5.33	-40.37	22.80	-12.18
May	-1.30	2.11	-52.50	52.10	0.42
June	-4.05	0.74	-51.28	78.94	24.35
July	-3.61	1.45	-41.08	94.86	51.62
August	-2.63	1.05	-42.35	61.70	17.78
September	-0.09	4.63	-39.95	9.75	-25.66
October	0.64	7.24	-34.89	0.03	-26.98
November	0.32	7.18	-34.81	0.00	-27.31
December	0.14	7.00	-34.13	0.00	-26.98
Net Annual	-9.88	60.75	-465.26	322.19	-92.20
Mean Monthly	-0.82	5.06	-38.77	26.85	-7.68

Central Arctic Turbulent and Thermodynamic Trends (W/m^2)					
	Latent Heat	Sensible Heat	Longwave	Shortwave	Net TTF Fluxes
January	0.07	-0.94	-5.62	0.00	-6.48
February	0.05	-0.57	-5.32	0.00	-5.84
March	-0.02	-1.06	-4.05	-0.01	-5.14
April	-0.08	-0.59	-2.04	-0.10	-2.81
May	-0.45	-0.08	0.01	0.86	0.34
June	-0.12	0.52	1.73	10.17	12.30
July	0.00	0.45	2.02	50.78	53.25
August	-1.41	-1.56	2.56	40.94	40.52
September	-4.54	-5.73	-4.48	10.14	-4.60
October	-0.52	-1.86	-11.24	0.01	-13.61
November	0.29	-0.78	-8.61	0.00	-9.11
December	0.17	-0.37	-7.32	0.00	-7.52
Net Annual	-6.55	-12.58	-42.36	112.80	51.31
Mean Monthly	-0.55	-1.05	-3.53	9.40	4.28

Barents Sea

Barents Sea Turbulent and Thermodynamic Climatology (W/m^2)					
	Latent Heat	Sensible Heat	Longwave	Shortwave	Net TTF Fluxes
January	-8.48	-16.77	-50.45	0.00	-75.70
February	-5.30	-8.78	-45.65	0.36	-59.37
March	-4.93	-7.42	-44.15	8.76	-47.75
April	-5.39	-6.13	-45.67	32.03	-25.18
May	-7.97	-5.38	-42.52	67.20	11.33
June	-7.82	-2.25	-32.37	113.17	70.73
July	-4.61	-0.40	-25.98	165.41	134.43
August	-7.67	-3.92	-24.76	111.93	75.58
September	-18.61	-13.02	-32.63	42.97	-21.28
October	-32.50	-32.86	-45.79	5.86	-105.30
November	-35.37	-51.47	-57.84	0.00	-144.68
December	-21.11	-37.20	-54.34	0.00	-112.64
Net Annual	-159.77	-185.62	-502.14	547.69	-299.84
Mean Monthly	-13.31	-15.47	-41.85	45.64	-24.99

Barents Sea Turbulent and Thermodynamic Trends (W/m^2)					
	Latent Heat	Sensible Heat	Longwave	Shortwave	Net TTF Fluxes
January	-30.94	-47.92	-9.85	0.00	-88.71
February	-18.30	-30.23	-7.55	0.21	-55.87
March	-9.45	-15.58	-3.62	3.37	-25.28
April	-5.50	-7.32	-1.82	12.00	-2.65
May	-2.81	-2.36	0.29	26.45	21.57
June	-0.33	-0.72	1.78	40.89	41.63
July	-1.40	-1.27	-0.13	19.75	16.95
August	-3.15	-0.85	-1.43	2.09	-3.35
September	-1.77	2.53	2.48	-1.45	1.79
October	-0.07	11.43	7.95	-0.32	18.99
November	-8.89	11.51	10.55	0.00	13.18
December	-29.19	-29.38	-2.95	0.00	-61.52
Net Annual	-111.81	-110.14	-4.30	102.99	-123.26
Mean Monthly	-9.32	-9.18	-0.36	8.58	-10.27

GIN Seas

Gin Seas Turbulent and Thermodynamic Climatology (W/m^2)					
	Latent Heat	**Sensible Heat**	**Longwave**	**Shortwave**	**Net TTF Fluxes**
January	-58.69	-104.98	-62.31	0.00	-225.97
February	-60.49	-106.77	-61.84	0.76	-228.34
March	-58.37	-101.91	-60.16	19.15	-201.28
April	-42.15	-66.83	-55.80	68.60	-96.18
May	-22.84	-25.79	-46.58	123.12	27.90
June	-8.90	-4.52	-23.59	135.81	98.82
July	-4.55	-0.67	-19.24	156.13	131.67
August	-9.20	-4.55	-22.19	104.57	68.63
September	-19.98	-14.97	-33.82	40.31	-28.46
October	-36.77	-41.64	-48.49	5.19	-121.71
November	-46.49	-72.57	-57.69	0.00	-176.75
December	-46.23	-76.44	-57.48	0.00	-180.15
Net Annual	-414.64	-621.65	-549.17	653.64	-931.82
Mean Monthly	-34.55	-51.80	-45.76	54.47	-77.65

GIN Seas Turbulent and Thermodynamic Trends (W/m^2)					
	Latent Heat	**Sensible Heat**	**Longwave**	**Shortwave**	**Net TTF Fluxes**
January	10.91	25.34	2.44	0.00	38.69
February	11.13	27.25	4.32	-0.02	42.69
March	8.22	19.14	2.75	-0.26	29.85
April	5.29	13.28	0.80	0.27	19.64
May	4.38	7.93	4.25	1.87	18.44
June	2.05	1.76	2.97	13.09	19.87
July	0.35	-0.03	-0.19	20.25	20.37
August	-0.32	0.67	-0.35	6.10	6.11
September	1.82	6.62	4.35	0.15	12.94
October	6.21	19.48	7.85	-0.13	33.41
November	2.99	21.20	3.52	0.00	27.71
December	4.63	19.16	1.84	0.00	25.62
Net Annual	57.66	161.78	34.56	41.32	295.33
Mean Monthly	4.81	13.48	2.88	3.44	24.61

Overall Arctic

Overall Arctic Turbulent and Thermodynamic Climatology (W/m^2)					
	Latent Heat	**Sensible Heat**	**Longwave**	**Shortwave**	**Net TTF Fluxes**
January	-8.02	-4.83	-37.97	0.01	-50.82
February	-7.49	-3.44	-36.26	1.15	-46.04
March	-6.64	-2.38	-37.64	10.71	-35.94
April	-5.73	-2.27	-44.06	35.49	-16.58
May	-7.30	-3.27	-47.64	70.28	12.08
June	-9.41	-4.67	-42.40	115.51	59.03
July	-9.82	-8.41	-37.63	148.06	92.19
August	-10.27	-6.56	-35.91	100.55	47.81
September	-11.46	-5.76	-41.22	39.88	-18.56
October	-12.88	-8.05	-42.92	6.59	-57.26
November	-10.49	-7.60	-42.12	0.15	-60.06
December	-8.24	-5.01	-39.29	0.00	-52.54
Net Annual	-107.75	-62.25	-485.05	528.36	-126.68
Mean Monthly	-8.98	-5.19	-40.42	44.03	-10.56

Overall Arctic Turbulent and Thermodynamic Trends (W/m^2)					
	Latent Heat	**Sensible Heat**	**Longwave**	**Shortwave**	**Net TTF Fluxes**
January	-1.56	-1.61	-3.83	0.00	-6.99
February	-0.97	-0.63	-2.80	0.04	-4.36
March	-0.66	-0.39	-1.76	0.32	-2.49
April	-0.65	-0.15	-0.73	1.36	-0.17
May	-0.47	0.47	0.65	4.47	5.11
June	-0.42	-0.36	1.35	17.99	18.57
July	-0.29	-0.60	1.42	23.96	24.49
August	-1.18	-0.70	2.62	12.98	13.73
September	-3.21	-1.14	2.16	6.05	3.86
October	-5.94	-2.90	-1.40	1.12	-9.11
November	-6.73	-5.71	-4.76	0.02	-17.18
December	-2.84	-3.29	-5.59	0.00	-11.72
Net Annual	-24.92	-17.01	-12.67	68.32	13.73
Mean Monthly	-2.08	-1.42	-1.06	5.69	1.14